



1 **ABSTRACT**

2 Previous studies have suggested that shading by riparian vegetation may reduce maximum  
3 water temperatures and provide refugia for temperature sensitive aquatic organisms.  
4 Longitudinal cooling gradients have been observed during the daytime for stream reaches  
5 shaded by coniferous trees downstream of clear cuts, or deciduous woodland downstream of  
6 open moorland. However, little is known about the energy exchange processes that drive such  
7 gradients, especially in semi-natural woodland contexts without confounding cool  
8 groundwater inflows. To address this gap, this study quantified and modelled variability in  
9 stream temperature and heat fluxes along an upland reach of the Girnock Burn (a tributary of  
10 the Aberdeenshire Dee, Scotland) where riparian landuse transitions from open moorland to  
11 semi-natural, predominantly deciduous woodland. Observations were made along a 1050 m  
12 reach using a spatially-distributed network of ten water temperature dataloggers, three  
13 automatic weather stations, and 211 hemispherical photographs that were used to estimate  
14 incoming solar radiation. These data parameterised a high-resolution energy flux model,  
15 incorporating flow-routing, which predicted spatio-temporal variability in stream  
16 temperature. Variability in stream temperature was controlled largely by energy fluxes at the  
17 water column-atmosphere interface. Net energy gains occurred along the reach,  
18 predominantly during daylight hours, and heat exchange across the bed-water column  
19 interface accounted for < 1% of the net energy budget. For periods when daytime net  
20 radiation gains were high (under clear skies), differences between water temperature  
21 observations increased in the streamwise direction; a maximum instantaneous difference of  
22 2.5 °C was observed between the upstream reach boundary and 1050 m downstream.  
23 Furthermore, daily maximum water temperature at 1050 m downstream was  $\leq 1$  °C cooler  
24 than at the upstream reach boundary and lagged by > 1 hour. Temperature gradients were not  
25 generated by cooling of stream water, but rather by a combination of reduced rates of heating  
26 in the woodland reach and advection of cooler (overnight and early morning) water from the  
27 upstream moorland catchment. Longitudinal thermal gradients were indistinct at night and on  
28 days when net radiation gains were low (under over-cast skies), thus when changes in net  
29 energy gains or losses did not vary significantly in space and time, and heat advected into the  
30 reach was reasonably consistent. The findings of the study and the modelling approach  
31 employed are useful tools for assessing optimal planting strategies for mitigating against  
32 ecologically damaging stream temperature maxima.

## 1. INTRODUCTION

River temperature dynamics are of increasing interest to the scientific community, environment managers and regulators (Hannah et al., 2008) given climate change predictions (e.g. van Vliet et al., 2011; Beechie et al., 2013) and associated consequences for water temperature and thereby aquatic ecosystems (Poole and Berman, 2001; Caissie, 2006; Webb et al., 2008; Wilby et al., 2010; Leach et al., 2012). Numerous studies have demonstrated that the presence of riparian woodland can decrease diurnal variability, mean and maximum stream temperatures (e.g. Malcolm et al., 2008; Brown et al., 2010; Roth et al., 2010; Imholt et al., 2012; Garner et al., 2014), or conversely that forest removal results in temperature increases (e.g. Macdonald et al., 2003; Rutherford et al., 2004; Danehy et al., 2005; Moore et al., 2005; Gomi et al., 2006). Consequently, there is substantial interest from researchers and stream managers in the potential of riparian vegetation to mitigate against climate change impacts (e.g. The River Dee Trust; Upper Dee Planting Scheme, 2011), especially in relation to thermal maxima.

Several studies have documented daytime cooling gradients (instantaneous decreases in downstream temperature) under forest canopies located downstream of open (no trees) landuse, although the magnitude of reported cooling effects varied between studies (e.g. Brown, 1971; Rutherford et al., 1997; McGurck 1989, Keith et al. 1998; Zwieniecki and Newton, 1999; Torgerson et al., 1999; Story et al., 2003; Westhoff et al., 2011). For example, McGurck (1989), Keith et al. (1998) and Story et al. (2003) observed gradients of between  $4.0\text{ }^{\circ}\text{C km}^{-1}$  and  $9.2\text{ }^{\circ}\text{C km}^{-1}$ . Little is known about the energy exchange processes that generate this apparent cooling effect (Story et al., 2003). Studies by Brown (1971) and Story et al. (2003) observed net energy gains to the water column measured predominantly across the air-water column interface. The presence of net energy gains lead both Brown (1971) and Story et al. (2003) to attribute the generation of cooling gradients to groundwater inputs that were thought to be underestimated by unrepresentative energy exchange measurements made at a single point within the reach (e.g. Brown, 1971; Story et al., 2003; Moore et al., 2005; Leach and Moore, 2011; Garner et al., 2014). Cooling gradients have also been observed in forested reaches downstream of open landuse in which groundwater inputs are considered to be minimal (e.g. Malcolm et al., 2004; Imholt et al., 2010; Imholt et al., 2012). However, an explicit conceptualisation of the processes driving observed patterns of cooling in forested reaches without groundwater inputs is lacking; this is essential if stream managers are to plan future riparian planting strategies that maximise benefits at minimal cost.

This study aims to quantify and model spatio-temporal variability in stream water temperature and heat fluxes for an upland reach of the Girnock Burn (a tributary of the Aberdeenshire Dee, Scotland) where riparian landuse transitions from open moorland to semi-natural forest, and in which stream temperature variability is driven largely by energy fluxes at the water column-atmosphere interface (i.e. not confounded by groundwater inflow). The specific objectives are:

1. To quantify the magnitude of instantaneous longitudinal water temperature gradients within the reach and identify the meteorological conditions under which the strongest and weakest gradients occur.

- 1        2. To explore the effect of changing riparian vegetation density on heat fluxes within the  
2        reach.
- 3        3. To understand, using a simple flow routing model in conjunction with a Lagrangian  
4        water temperature model, how water temperature changes as it travels through the  
5        forested reach and attribute this to underlying processes.

## 6    **2. STUDY AREA**

7    A 1050 m study reach with no tributary inputs was established within Glen Girnock, an  
8    upland basin that drains into the Aberdeenshire Dee, northeast Scotland. Upstream of the  
9    reach ( $\sim 24 \text{ km}^2$ ), landuse is dominated by heather (*Calluna*) moorland. Within the reach  
10   landuse transitions from open moorland to semi-natural forest composed of birch (*Betula*),  
11   Scots pine (*Pinus*), alder (*Alnus*) and willow (*Salix*) (Imholt et al., 2012).

12   Full details of the Girnock catchment characteristics are found in Tetzlaff et al. (2007). In  
13   brief, soils are composed primarily of peaty podsoles with a lesser coverage of peaty gleys.  
14   Granite at higher elevations and schists at lower elevations dominate the geology, both of  
15   which have relatively impermeable aquifer properties (Tetzlaff et al., 2007). The riverbed in  
16   the study reach is composed primarily of cobble and boulder, with smaller patches of  
17   localised gravel accumulation. Previous work in the catchment suggests highly heterogeneous  
18   but spatially constrained groundwater discharge, with no significant groundwater inputs  
19   within the study reach (Malcolm et al., 2005). Thus in the absence of major groundwater  
20   inflow, heat exchange within the reach is dominated by fluxes at the water column-  
21   atmosphere interface. The Girnock Burn flows in a mainly northerly direction and so  
22   experiences no significant changes in aspect that may influence solar radiation receipt  
23   through topographic or bank shading (Figure 1). Maximum and minimum elevations of the  
24   reach are 280 m and 255 m respectively (Figure 1). Mean wetted width was 9.5 m during the  
25   study period.

## 26   **3. METHODS**

### 27   **3.1. Experimental design**

28   Ten water temperature loggers were deployed throughout a 1050 m reach of the Girnock  
29   where riparian landuse transitions from open moorland to semi-natural forest (Figure 1), and  
30   in which previous studies have identified measurable changes in stream temperature (e.g.  
31   Malcolm et al., 2004; Malcolm et al., 2008; Imholt et al., 2010; Imholt et al., 2012). Three  
32   automatic weather stations (AWSs) were deployed along the reach to estimate spatio-  
33   temporal variability in energy fluxes: one in open moorland (AWS<sub>open</sub>) and two in semi-  
34   natural forest (AWS<sub>FUS</sub> followed by AWS<sub>FDS</sub>). The number and location of AWSs was  
35   limited by logistical and financial constraints. However, 211 hemispherical photographs were  
36   taken at 5 m intervals along the reach so that solar radiation measured at the open site AWS  
37   could be re-scaled to estimate radiative fluxes at a higher spatial resolution. For locations  
38   where hemispherical images were taken, turbulent (i.e. latent and sensible heat) and bed heat  
39   fluxes were estimated by linearly interpolating between values at the two nearest AWSs.

1 High-resolution information on energy fluxes and stream temperature was combined with a  
2 flow-routing model to provide process-based understanding of spatio-temporal variability in  
3 stream temperature.

### 4 **3.2 Data collection**

5 Field data were collected between October 2011 and July 2013. A seven-day period (1 to 7  
6 July 2013) characterised by high air temperatures (i.e. > average air temperatures for this  
7 week in the preceding ten years) and extremely low flows (i.e. < average minimum flows for  
8 this week in the preceding ten years) was chosen to meet the aims of the study (Figure 2).  
9 High energy gains occurred on six days and relatively low energy gains occurred on one day.  
10 These data allowed assessment of: (1) potential mitigation of high temperatures by semi-  
11 natural forest under a ‘worst case scenario’ of high energy gains and low flows; and (2) the  
12 influence of contrasting prevailing meteorological conditions on longitudinal water  
13 temperature patterns.

#### 14 *3.2.1. Stream temperature measurements*

15 Stream temperature measurements were made at 15-minute intervals across a spatially-  
16 distributed network of ten water temperature TinyTag Aquatic 2 dataloggers (manufacturer  
17 stated accuracy of +/- 0.5 °C) and three Campbell 107 thermistors (manufacturer stated  
18 accuracy +/- 0.1 °C) connected to AWSs at 0 (AWS<sub>Open</sub>), 190, 315, 460, 565, 630, 685  
19 (AWS<sub>FUS</sub>), 760, 815, 865, 940 1015 and 1050 (AWS<sub>FDS</sub>) m downstream of the upstream  
20 reach boundary (i.e. AWS<sub>Open</sub>) (Figure 1). The sensors were cross-calibrated (Hannah et al.,  
21 2009) prior to installation and showed good agreement (i.e. < +/- 0.1 °C over the range 0-30  
22 °C). Within the reach, sensors were housed in white plastic PVC tubes to shield them from  
23 direct solar radiation.

#### 24 *3.2.2. Hydrology and stream geometry*

25 Flow accretion surveys (following the velocity-area method) were conducted at 200 m  
26 intervals along the reach to assess net flow gains and losses between the channel and  
27 subsurface (Leach and Moore, 2011). No significant gains or losses of discharge were  
28 observed, with differences between gaugings consistently within +/- 10% of each other (i.e.  
29 within velocity –area measurement uncertainty; Leach and Moore, 2011). These gaugings  
30 supported previous stream and streambed hydrochemical surveys (e.g. Malcolm et al., 2005)  
31 that suggested groundwater gains along the reach were negligible. Given the very significant  
32 methodological and logistical challenges in obtaining realistic hyporheic flux estimates over  
33 such a large spatial extent neither volumes, flow path lengths, or the distribution of residence  
34 times of potential hyporheic exchange were quantified.

35 A Scottish Environmental Protection Agency (SEPA) gauging station at Littlemill (Figure 1)  
36 provided discharge data at 15-minute intervals. The discharge- mean velocity function for  
37 Littlemill presented in Tetzlaff et al. (2005) was used to calculate water velocity and thus  
38 drive the flow-routing model. Good correspondence was observed between velocities and  
39 discharges measured during flow accretion surveys and those calculated from discharge at  
40 Littlemill scaled (linearly) by catchment area. Wetted width was measured at 50 m intervals  
41 along the reach and used as input to the water temperature model.

### 1 3.2.3. Micrometeorological measurements

2 Three automatic weather stations (AWSs) were installed within the reach (Figure 1). The  
3 instruments deployed on the AWSs are detailed in Hannah et al. (2008). Measured  
4 hydrometeorological variables included air temperature ( $^{\circ}\text{C}$ ), relative humidity (%), wind  
5 speed ( $\text{ms}^{-1}$ ), incoming solar radiation, net radiation and bed heat flux (all  $\text{Wm}^{-2}$ ).  
6 Meteorological measurements were made  $\sim 2$  m above the stream surface. The bed heat flux  
7 plate was located directly below each AWS and buried at 0.05 m depth to avoid radiative and  
8 convective errors (after Hannah et al., 2008). The heat flux plate provided aggregated  
9 measurements of convective, conductive, advective and radiative heat exchanges between the  
10 atmosphere and the riverbed, and the riverbed and the water column (after Evans et al., 1998;  
11 Hannah et al., 2008). All sensors were cross-calibrated prior to installation and correction  
12 factors applied if required. The sensors were sampled at 10-second intervals, with averages  
13 logged every 15-minutes.

### 14 3.2.4. Hemispherical images

15 Hemispherical images were taken at 5 m intervals along the stream centreline using a Canon  
16 EOS-10D 6.3 megapixel digital camera with Sigma 8 mm fisheye lens. Prior to taking each  
17 image the camera was orientated to north and levelled  $\sim 20$  cm above the stream surface (after  
18 Leach and Moore, 2010).

## 19 3.3. Estimation of stream energy balance components

### 20 3.3.1. Net energy

21 Net energy ( $\text{Wm}^{-2}$ ) available to heat or cool the water column was calculated as:

$$22 Q_n = Q^* + Q_e + Q_h + Q_{bhf} \text{ (Equation 1)}$$

23 Where  $Q_n$  is net energy,  $Q^*$  is net radiation,  $Q_e$  is latent heat,  $Q_h$  is sensible heat **and  $Q_{bhf}$  is**  
24 **bed heat flux** (all  $\text{Wm}^{-2}$ ). Heat from fluid friction is negligible in this reach (see Garner et al.,  
25 2014) and was therefore omitted. Herein, energy fluxes are considered to be positive  
26 (negative) when directed toward (away from) the water column.

### 27 3.3.2. Net radiation

28 A deterministic model developed by Moore et al. (2005) and evaluated by Leach and Moore  
29 (2010) was used to compute net radiation ( $Q^*$ ) at the location of each hemispherical image.  
30 At each location net radiation was calculated as:

$$31 Q^* = K^* + L^* \text{ (Equation 2)}$$

32 Where  $K^*$  is net shortwave radiation (Equation 3) and  $L^*$  is net longwave radiation (Equation  
33 4).

$$34 K^* = (1 - \alpha)[D(t)g(t) + s(t)f_v] \text{ (Equation 3)}$$

$$35 L^* = [f_v \varepsilon_a + (1 - f_v) \varepsilon_{vt}] \sigma (T_a + 273.2)^4 - \varepsilon_w \sigma (T_w + 273.2)^4 \text{ (Equation 4)}$$

1 Where  $\alpha$  is the stream albedo,  $D(t)$  is the direct component of incident solar radiation at time  $t$   
 2 ( $\text{Wm}^{-2}$ ),  $g(t)$  is the canopy gap fraction at the position of the sun in the sky at time  $t$ ,  $S(t)$  is the  
 3 diffuse component of solar radiation,  $f_v$  is the sky view factor,  $\epsilon_a$ ,  $\epsilon_{vt}$  and  $\epsilon_w$  are the emissivity  
 4 of the temperatures of the air, vegetation and water respectively (all  $^{\circ}\text{C}$ ),  $\sigma$  is the Stefan-  
 5 Boltzmann constant ( $5.67 \times 10^{-8} \text{ Wm}^{-2} \text{ K}^{-4}$ ), and  $T_a$  and  $T_w$  are air and water temperature  
 6 respectively (both  $^{\circ}\text{C}$ ).

7 Values for atmospheric emissivity were calculated for clear-sky day and night conditions  
 8 using the equation presented in Prata (1996; used also by Leach and Moore, 2010) and were  
 9 subsequently adjusted for cloud cover using equations in Leach and Moore (2010). The  
 10 emissivity and albedo were taken to be 0.95 and 0.05 for water, and 0.97 and 0.03 for  
 11 vegetation respectively (after Moore et al., 2005; Leach and Moore, 2010).

12 Gap fractions ( $g_*$ ) were computed as a function of solar zenith angle ( $\theta$ ) and solar azimuth  
 13 ( $\psi$ ),  $g_*(\theta, \psi)$ , which were derived from analysis of the hemispherical images with Gap Light  
 14 Analyser software (Frazer et al., 1999). The optimum threshold value for converting the  
 15 hemispherical photographs into binary images was calculated in three steps (after Leach and  
 16 Moore, 2010): (1) threshold values of 120 to 190 at 10 unit increments were applied to the  
 17 photographs taken at  $\text{AWS}_{\text{FUS}}$ , (2) for each threshold value, incoming shortwave radiation  
 18 was modelled at 15 minute intervals across the seven day study period, and (3) modelled time  
 19 series were compared quantitatively with values measured at  $\text{AWS}_{\text{FUS}}$  by calculating RMSE.  
 20 A threshold value of 130 minimised RMSE and was thus identified as the optimum. It was  
 21 assumed that this threshold value was optimum throughout the reach and was applied to all  
 22 211 hemispherical photographs. This assumption was reasonable because all photographs  
 23 were taken on the same day during which sky conditions were consistently overcast. Using  
 24 equations in Iqbal (1983), the solar zenith and azimuth angles were computed as a function of  
 25 time,  $t$ , so that the canopy gap at the location of the sun's disk could be derived from  $g_*(\theta, \psi)$   
 26 as a function of time  $g(t)$ . Sky view factor was computed as:

$$27 \quad f_v = \frac{1}{\pi} \int_0^{2\pi} \int_0^{\pi/2} g_*(\theta, \psi) \cos \theta \sin \theta * d\theta * d\psi$$

28 (Equation 5)

29 The double integral was approximated by summation using an interval of  $5^{\circ}$  for both solar  
 30 zenith and azimuth angles (after Leach and Moore, 2010). Solar radiation measurements  
 31 made at  $\text{AWS}_{\text{open}}$  were used as input to the radiation models. Modelled and observed values  
 32 of incoming solar radiation were compared at each AWS for the entire study period; RMSE  
 33 ( $< 75 \text{ Wm}^{-2}$ ) compared favourably with those observed by Leach and Moore (2010).

### 34 3.3.3. Latent and sensible heat fluxes

35 To compute heat lost by evaporation or gain by condensation, latent heat was estimated after  
 36 Webb and Zhang (1997) (Equation 6).

$$37 \quad Q_e = 285.9(0.132 + 0.143 * U)(e_a - e_w)$$

38 (Equation 6)

1 Where  $U$  is wind speed ( $\text{ms}^{-1}$ ) and  $e_a$  and  $e_w$  are vapour pressures of air and water (both kPa),  
2 respectively.

$$3 \quad e_{sat}(T) = 0.611 * \exp \left[ \frac{2.5 * 10^6}{461} * \left( \frac{1}{273.2} - \frac{1}{T} \right) \right]$$

4 (Equation 7)

5 Vapour pressure of water ( $e_w$ ) was assumed to be equal to  $e_{sat}(T_w)$ . Vapour pressure of air was  
6 calculated using Equation 8.

$$7 \quad e_a = \frac{RH}{100} e_{sat}(T_a) \text{ (Equation 8)}$$

8 Sensible heat (Equation 9) was calculated as a function of latent heat (Equation 6) and Bowen  
9 ratio ( $\beta$ ) (Equation 10), where  $P$  is air pressure (kPa).

$$10 \quad Q_h = Q_e * \beta \text{ (Equation 9)}$$

$$11 \quad \beta = 0.66 * \left( \frac{P}{1000} \right) * [(T_w - T_a) / (e_a - e_w)] \text{ (Equation 10)}$$

## 12 **3.4. Modelling approaches**

### 13 *3.4.1. Statistical models*

14 Spatial (and temporal) variability in canopy density (and net energy flux) was extremely high.  
15 Therefore, in order to characterise broad patterns in space (and time) generalised additive  
16 models (GAMs; Hastie and Tibshirani, 1986) were used to provide continuous smoothed  
17 estimates of the variability in each dataset. GAMs were fitted in the MGCV package (Wood,  
18 2006; version 1.7-13) for R (R Group for Statistical Computing; version 3.0.2). Degrees of  
19 freedom were obtained by generalised cross-validation within the MGCV library but were  
20 limited in order to prevent over-fitting by setting ‘gamma’ to 1.4 following Wood (2006).

21 The GAM fitted to canopy density provided a continuous smoothed estimate of the spatial  
22 variability in density from discrete (5 m interval) point measurements determined from Gap  
23 Light Analyser outputs. Canopy density was calculated as the percentage of pixels  
24 representative of vegetation in each hemispherical image; this percentage was modelled as a  
25 smoothed function of distance downstream (i.e. from  $\text{AWS}_{\text{Open}}$ ).

26 The second GAM provided a continuous smoothed estimate of the spatio-temporal variability  
27 in net energy flux estimated at 5 m intervals from the sum of scaled radiative flux (see  
28 Section 4.4.3), and turbulent and bed heat fluxes calculated from hydrometeorological  
29 observations scaled by linear interpolation between the two nearest AWSs. Specifically, net  
30 energy was modelled as smoothed functions of: (i) time of day, (ii) day of year, and (iii)  
31 distance downstream. The inclusion of three smoothed terms was validated by fitting models  
32 using each combination of the three terms and comparing each using AIC (Akaike  
33 information criterion; Burnham and Anderson, 2002) score, a measure of model quality that  
34 balances fit and parsimony, between models. The selected model was that with the lowest  
35 AIC, since there were no other candidate models (within an AIC of 2 of the selected model).



### 1 3.4.2. Flow routing model

2 A flow routing model was used to predict the time taken by water parcels to travel through  
3 the reach. The model was based on a discharge- mean velocity function (Tetzlaff et al., 2005)  
4 and predicted the distance travelled by water parcels at 15-minute intervals. In combination  
5 with the dataset of spatio-temporally distributed water temperature observations, the model  
6 also identified the temperature of distinct water volumes at 15-minute intervals.

7 The model released water from  $AWS_{open}$  at the start of every hour on each day of the study  
8 period. For each parcel of water ( $i$ ) the distance travelled in 15 minutes from its initial  
9 location ( $x$ ) to the next location ( $x+I$ ) was calculated as the product of the length of the  
10 timestep ( $\Delta t$ , i.e. 900 seconds) and the average velocity at times  $t$  and  $t+\Delta t$ . The temperature  
11 of the parcel at location  $x+I$  and time  $t+\Delta t$  was determined by linear interpolation (to the  
12 nearest 1 m) between measurements at 15 minute intervals and between temperature loggers,  
13 respectively.

### 14 3.4.3. Lagrangian water temperature model

15 The Lagrangian modelling approach (after Bartholow, 2000; Boyd and Kasper, 2003;  
16 Rutherford et al., 2004; Westhoff et al., 2007, 2010; Leach and Moore, 2011; MacDonald et  
17 al., 2014a, 2014b) divided the reach into a series of segments ( $s$ ) bounded by nodes (indexed  
18 by  $j$ ). For each time step,  $\Delta t$  (i.e. 900 seconds), a water parcel ( $i$ ) was released from the  
19 upstream boundary; its initial temperature was an observed value. As the water parcel  
20 travelled downstream from  $j$  towards  $j+I$  the model computed the heat exchange and the net  
21 change in stream temperature over the segment as the mean of net energy flux within the  
22 segment at time  $t$  and time  $t+ \Delta t$  (Equation 10).

$$\frac{dT_w}{dx} = \frac{\left[ \frac{w_{(s)}(K^*_{(s,t)} + L^*_{(s,t)} + Q_{h(s,t)} + Q_{e(s,t)} + Q_{bhf(s,t)})}{w_{(s)}(K^*_{(s,t+\Delta t)} + L^*_{(s,t+\Delta t)} + Q_{h(s,t+\Delta t)} + Q_{e(s,t+\Delta t)} + Q_{bhf(s,t+\Delta t)})} \right] / 2}{C [(F_{(s,t)} + F_{(s,t+\Delta t)}) / 2]}$$

23 (Equation 10)

24 Where  $W_{(s)}$  is the mean wetted width of the stream surface (m) within segment  $s$ ,  $K^*_{(s,t+\Delta t)}$ ,  
25  $L^*_{(s,t+\Delta t)}$ ,  $Q_{e(s,t+\Delta t)}$ ,  $Q_{h(s,t+\Delta t)}$  and  $Q_{bhf(s,t+\Delta t)}$  are the mean net shortwave, net longwave,  
26 latent, sensible and bed heat fluxes within segment  $s$  at time  $t$  or  $t+\Delta t$ .  $C$  is the specific heat  
27 capacity of water ( $4.18 \times 10^6 \text{ J m}^{-3} \text{ }^\circ\text{C}^{-1}$ ) and  $F_{(s,t+\Delta t)}$  is the discharge ( $\text{m}^3\text{s}^{-1}$ ; scaled by  
28 catchment area) within segment  $s$  at time  $t$  or  $t+\Delta t$

29 Water temperature was calculated at 1 m intervals along the reach by integration of Equation  
30 10 in the deSolve package (Soetaert et al., 2010) for R (Version 3.0.2, R Group for Statistical  
31 Computing, 2013).

32 Unsmoothed (raw) energy flux data were used for numerical modelling. Incident solar  
33 radiation was modelled at 5 m intervals (see section 4.4.3, *Net radiation*); values at 1 m  
34 intervals were obtained by linear interpolation. Emitted longwave radiation, latent and  
35 sensible heat fluxes were dependent on water temperature. Therefore, these fluxes were  
36 calculated at each time step within Equation 10 using values for air temperature, humidity

1 and wind speed estimated at 1 m intervals by linear interpolation between the two nearest  
2 AWSs.

### 3 *3.3.4 Sensitivity analysis*

4 With the exception of the threshold value applied to the hemispherical images (see Section  
5 3.3.2) no site-specific parameters were used for water temperature modelling. A sensitivity  
6 analysis was conducted on the image threshold parameter to assess its influence on water  
7 temperature model output. Time series of incident shortwave radiation modelled at AWS<sub>FUS</sub>  
8 using the assumed maximum (i.e. 190) and minimum (i.e. 120) thresholds were retained  
9 during the procedure described in Section 3.3.2. Percentage changes in incident shortwave  
10 radiation between the optimum (130) and assumed maximum and minimum values were  
11 calculated for 15 minute intervals across the entire study period. The percentage changes  
12 associated with the upper and lower thresholds were used to generate two datasets of incident  
13 shortwave radiation representative of potential maximum and minimum values. This assumed  
14 that percentage changes calculated at AWS<sub>FUS</sub> were representative of changes throughout the  
15 entire reach; this was a reasonable assumption given that all photographs were taken on the  
16 same day, during which sky conditions remained overcast. To quantify the effect of the  
17 threshold on model outputs, two additional model runs were performed for each water parcel  
18 released from AWS<sub>Open</sub> using each of these datasets of incident solar radiation.

## 19 **4. RESULTS**

20 Results are presented in four sections: (1) prevailing **hydrological and** weather conditions, (2)  
21 observed spatio-temporal water temperature patterns, (3) riparian canopy density and net  
22 energy flux patterns, and (4) modelled spatio-temporal water temperature patterns.

### 23 **4.1. Prevailing hydrological and weather conditions**

24 A total of 4.2 mm of rain was measured in the catchment during the study period  
25 (01/07/2013- 07/07/2013). Stream discharge measured at Littlemill was very low (0.074-  
26 0.138 m<sup>3</sup>s<sup>-1</sup>), reasonably stable, and exhibited no sudden changes (Figure 2). **Days** 01/07,  
27 03/07, 04/07, 05/07, 06/07 and 07/07 were characterised by high net energy gains to the water  
28 column during daylight hours, driven by clear-skies and consequently high solar radiation  
29 receipt (Figure 2). On 02/07 net energy gains were markedly lower due to overcast skies and  
30 associated low solar radiation receipt (Figure 2). This data window allowed investigation of  
31 the influence of contrasting energy gain conditions (i.e. low versus high net energy gain) on  
32 the spatio-temporal variability of water temperature and energy flux.

### 33 **4.2. Observed spatio-temporal water temperature patterns**

34 Instantaneous longitudinal temperature gradients occurred frequently throughout the entire  
35 monitoring period (Figure 3). Gradients were greatest in spring and summer months during  
36 which time warming gradients were much smaller (< 0.5 °C) than cooling gradients (≤ 2.5  
37 °C). Gradients were especially large during the chosen 7-day study period.

38 During the study period, minimum daily water temperature was the same at both AWS<sub>Open</sub>  
39 and AWS<sub>FDS</sub> (9.8 °C) but maximum temperature was higher at AWS<sub>Open</sub> than at AWS<sub>FDS</sub>,

1 with observed temperatures of 23.0 °C and 22.0 °C, respectively (both occurring on 06/07)  
2 (Figure 2f). Minimum temperatures occurred synchronously across all three locations (Figure  
3 2f). Maximum temperatures at AWS<sub>FDS</sub> lagged those at AWS<sub>Open</sub> by between 1 hour and 1.75  
4 hours on all days except 02/07 (Figure 2f). On 02/07 when skies were overcast and the water  
5 column received lower solar radiation, maximum temperatures occurred synchronously at  
6 both locations (Figure 2f).

7 Longitudinal gradients in instantaneous water temperature measurements (at a particular  
8 point in time across the entire reach) were observed during daylight hours on each day of the  
9 study period. Instantaneous water temperatures were greatest at AWS<sub>Open</sub> and decreased  
10 downstream towards AWS<sub>FDS</sub>. Large daily temperature amplitudes (Figure 4a) and distinct  
11 downstream gradients of > 1 °C (Figure 4b) were observed on 01/07, 03/07, 04/07, 05/07,  
12 06/07 and 07/07 between 11:00 and 16:00 GMT. The greatest instantaneous temperature  
13 gradient was 2.5 °C in magnitude, observed on 06/07 at 12:00 (Figure 4b). On 02/07, the  
14 amplitude of the diurnal water temperature cycle was greatly reduced (Figure 4a) and  
15 longitudinal water temperature gradients were small (Figure 4b) with the greatest gradient  
16 (0.6 °C) observed at 08:00 GMT, and smaller gradients (< 0.2 °C i.e. below measurement  
17 accuracy of the sensors) observed between 11:00 and 15:00 GMT (Figure 4b).

18 Overnight, longitudinal gradients were reversed (*cf.* daylight hours); instantaneous water  
19 temperatures were lowest at AWS<sub>Open</sub> and increased downstream towards AWS<sub>FDS</sub> (Figure  
20 4b). However, the difference in temperature between these two sites during the night was  
21 consistently < 0.5 °C in magnitude.

### 22 **4.3. Riparian canopy density and net energy flux patterns**

23 Between AWS<sub>Open</sub> (0 m) and 400 m patchy forest cover (Figures 5a and 5b) generated canopy  
24 densities ranging from 0.0 % to 70.3 % (Figure 6a). Between 400 m and 1050 m (AWS<sub>FDS</sub>)  
25 continuous riparian forest of variable density (Figures 5c and 5d) produced typically lower  
26 but still variable gap fractions ranging from 22.5 % to 92.0 % (Figure 6a). The forest canopy  
27 was densest between 400 m and 800 m and decreased in density between 800 m and 1050  
28 Figure 6a).

29 The spatial variability in net energy corresponded broadly to canopy density (Figure 6). Net  
30 energy gains during daylight hours decreased gradually from AWS<sub>Open</sub> to 400 m before  
31 declining sharply between 400 m and 800 m. Between 800 m and 1050 m (AWS<sub>FDS</sub>), net  
32 energy flux increased markedly. Strong diurnal signals and distinct spatial patterns were  
33 observed during daylight hours on 01/07, 03/07, 04/07, 05/07, 06/07 and 07/07, with spatial  
34 patterns especially clear around solar noon (Figure 6b). On 02/07, the spatial and temporal  
35 variability of net energy fluxes was much subdued. Around solar noon on 02/07, net energy  
36 flux was slightly lower at 800 m but differences within the reach were otherwise  
37 indistinguishable (Figure 6b), driven by smaller differences (relative to clear sky conditions)  
38 in solar radiation gain between open and forested sites (Figure 2c to 2e).

39 During the night, small and temporally consistent differences in net energy occurred within  
40 the reach (Figure 6b). Net energy losses were greatest at AWS<sub>Open</sub> and declined up until 400

1 m before stabilising and increasing again between 800 m and 1050 m, yet spatial variability  
2 was markedly reduced in comparison to daytime conditions on 01/07, and 03/07- 07/07.

#### 3 **4.4. Modelled spatio-temporal water temperature patterns**

4 The flow routing model (and associated observations of the temperature of water parcels as  
5 they travelled through the reach) was evaluated by predicting the change in temperature of  
6 water parcels (using the water temperature model). Temperature changes over the reach were  
7 compared with those predicted for water leaving AWS<sub>open</sub> (0 m, the upstream boundary of the  
8 reach) at 06:00, 07:00, 08:00 and 09:00 GMT. Water parcels released at these times were  
9 associated with the greatest observed instantaneous cooling gradients on arrival at the  
10 downstream reach boundary. Predictions of downstream temperature change (Figures 7 and  
11 8) were typically good, as indicated by: high  $R^2$  (ranging from 0.71 on 02/07 to 0.99 on  
12 06/07), and low RMSE (ranging from 0.2 °C on 01/07 and 02/07 to 0.4 °C on 07/07). Thus,  
13 the evaluation statistics compared favourably to those observed in previous studies using  
14 similar models (e.g. Westhoff et al., 2011). The model was biased towards slight over-  
15 prediction (as indicated by percent-bias) but in all cases this was < 2.0 %. Importantly, the  
16 model was capable of predicting instantaneous longitudinal cooling gradients with reasonable  
17 accuracy (i.e. +/-  $\leq 0.5$  °C) and the error in predicted gradients displayed no consistent bias.  
18 The sensitivity analysis on the threshold value for image processing demonstrated that the  
19 optimum threshold resulted in conservative predictions of downstream cooling. Higher  
20 threshold values (i.e. 140-190) resulted in much lower modelled temperatures at the  
21 downstream boundary (up to 0.9 °C) and consequently enhanced cooling gradients. A lower  
22 threshold (i.e. 120) increased modelled temperatures and therefore reduced modelled cooling  
23 gradients slightly, by up to 0.2 °C at the downstream reach boundary (Figure 8).

24 Using the flow routing model, the time taken for water to travel 1050 m through the reach  
25 from AWS<sub>Open</sub> to AWS<sub>FDS</sub> averaged 7.5 hours. Typically, water travelling from the upstream  
26 boundary of the reach between 01:00 and 12:00 GMT warmed as it travelled through the  
27 reach while water beginning its journey through the reach between 13:00 GMT and 00:00  
28 GMT cooled (Figure 8). On 01/07, 03/07, 04/07, 05/07, 06/07 and 07/07 water warmed  
29 between 4.2 °C and 6.9 °C while travelling through the reach; but, at the time of arrival at  
30 AWS<sub>FDS</sub>, it was cooler than the water temperature observed at AWS<sub>open</sub> at the same time. For  
31 example, on 06/07 the temperature of water leaving AWS<sub>open</sub> at 08:00 GMT was 14.3 °C.  
32 This water passed through the reach and arrived at AWS<sub>FDS</sub> at 15:30 GMT, by which time its  
33 temperature had risen to 20.1 °C. The water leaving AWS<sub>open</sub> at 15:30 GMT had a  
34 temperature of 21.2 °C (Figure 9a). Thus at 15:30 GMT, the water at AWS<sub>FDS</sub> was 1.1 °C  
35 cooler than that at AWS<sub>open</sub>. Distinct instantaneous cooling gradients were not observed on  
36 02/07, when water warmed < 1.5 °C while travelling through the reach. The water travelling  
37 from AWS<sub>open</sub> on day two at 07:00 GMT had a temperature of 10.4 °C and reached AWS<sub>FDS</sub>  
38 at 14:15 GMT attaining a temperature of 11.8 °C. Water travelling downstream from  
39 AWS<sub>open</sub> at 14:15 GMT also had a temperature of 11.8 °C and thus no cooling gradient was  
40 observed (Figure 9b).

## 1 **5. DISCUSSION**

2 This study has quantified longitudinal water temperature patterns in a stream reach where  
3 landuse transitions from open moorland to semi-natural forest. Furthermore, the riparian  
4 landuse controls and associated energy exchange and water transport processes that generate  
5 water temperature patterns have been identified. Significant groundwater inflows do not  
6 occur within the reach and thus energy exchange was dominated by fluxes at the air-water  
7 column interface, allowing an unconfounded conceptual understanding of the processes of  
8 longitudinal stream water cooling gradients under forest canopies. The following discussion  
9 identifies the key drivers and processes, their space-time dynamics, and the limitations of the  
10 study.

### 11 **5.1. Micrometeorological and landuse controls on energy exchange and water** 12 **temperature**

13 During daylight hours, the observation of net energy gains corroborated the observations of  
14 Brown et al. (1971), Story et al. (2003) and Westhoff et al. (2010) for shaded streams  
15 downstream of clearings. Distinctive longitudinal patterns of net energy exchange were  
16 observed on days with clear skies when solar radiation, and net energy gains were greatest;  
17 whereas net energy varied little within the reach on overcast days, indicating that  
18 meteorological conditions were a first-order control on patterns of net energy flux  
19 (Rutherford et al., 1997; 2004). The density of the semi-natural riparian forest canopy was a  
20 second order control on net energy flux. On days with clear skies, net energy gain was  
21 greatest where trees were absent (Moore et al., 2005) or the canopy was sparse, and least  
22 where the canopy was densest (Leach and Moore, 2010), owing to the canopy providing  
23 shading from solar radiation (Beschta and Taylor, 1988; Macdonald et al., 2003; Malcolm et  
24 al., 2004; Moore et al., 2005; Hannah et al., 2008; Imholt et al. 2010; 2012).

25 Contrasting meteorological conditions, and thus net energy gain conditions within the study  
26 period drove differences in the timing and magnitude of water temperature dynamics  
27 (Malcolm et al., 2004) and gradients observed within the reach. On overcast days, within-  
28 reach differences in the magnitude (Johnson and Jones, 2000) and timing of maximum daily  
29 temperatures, and longitudinal water temperature gradients were indistinguishable. However,  
30 on clear sky days, maximum daily temperatures decreased between the upstream and  
31 downstream reach boundary by up to 1 °C; locations further downstream experienced  
32 maximum temperatures later in the day and instantaneous cooling gradients of up to 2.5 °C  
33 (equivalent to 2.4 °C km<sup>-1</sup>) were observed. These decreases in temperature were much less  
34 than those observed by McGurck (1989), Keith et al. (1998), and Story et al. (2003) who  
35 observed instantaneous cooling gradients of between 4.0 °C km<sup>-1</sup> and 9.2 °C km<sup>-1</sup>. Variability  
36 in cooling gradients at and between sites may be attributed to differing climatic zones,  
37 prevailing weather conditions (Rutherford et al., 2004), riparian vegetation density and  
38 orientation, channel orientation and subsurface hydrology; all control the magnitude of  
39 energy exchange and consequently water temperature (Poole and Berman, 2001; Webb and  
40 Zhang, 1997).

## 1 **5.2. Alternative conceptualisation of processes generating longitudinal water** 2 **temperature gradients in forested river reaches**

3 The water temperature model reproduced downstream temperature patterns with a high level  
4 of accuracy using physically realistic parameters scaled from numerous local  
5 micrometeorological and river flow measurements. This suggests that the energy balance was  
6 near closed. Previous studies (e.g. Story et al., 2003) observed net energy gains to the water  
7 column (which cannot drive cooling of water as it travels downstream; Story et al., 2003); but  
8 they were conducted in river reaches with known cooler groundwater inflows and hyporheic  
9 exchanges. There are considerable challenges in identifying and quantifying volumes and  
10 temperatures of these spatially and temporally heterogeneous heat and water fluxes (see 5.3  
11 Limitations), and consequently of obtaining field measurements which close the energy  
12 budget. Therefore, these studies conceptualised high groundwater and hyporheic exchange  
13 contributions that enabled downstream cooling to be invoked in the models developed.  
14 Consequently, this work inferred that water cooled as it travelled downstream due to  
15 substantial cool groundwater inputs rather than spatial differences in energy exchanges at the  
16 water column-atmosphere beneath the forest canopy. The present study has demonstrated that  
17 cooling gradients may be produced in the absence of groundwater inputs in a shaded stream  
18 reach downstream of open landuse. Consequently, it presents an alternative conceptualisation  
19 of the processes that may generate spatio-temporal water temperature patterns. An important  
20 distinction between this research and other process explanations of instantaneous cooling  
21 gradients is that water does not need to cool as it travels downstream beneath a forest canopy.  
22 Instead, water can warm as it travels downstream but cooling gradients may be generated  
23 when the temperature of water advected into the reach increases over the day, while this  
24 water is subsequently heated minimally while flowing beneath the forested canopy.

25 Our results suggest that the following alternative process conceptualisation may generate  
26 spatio-temporal water temperature patterns in the absence of groundwater inflows on: (i) a  
27 clear sky day and (ii) an overcast sky day. On clear sky days, net energy fluxes increase  
28 reasonably consistently between sunrise and solar noon, driven by increasing solar radiation  
29 receipt. Consequently, the temperature of water crossing the upstream boundary of the study  
30 reach between sunrise and solar noon increases continually (i.e. more heat is advected into  
31 the reach) (Westhoff et al., 2010). On entering the forest, water temperature continues to  
32 increase but at a much reduced rate (Rutherford et al., 2004), as solar radiation and thus net  
33 energy are reduced considerably. Consequently, when net energy gains occur, water flowing  
34 through the forest is consistently cooler than water travelling through the upper reach and  
35 moorland during the same time. On overcast days, net energy gains increase little between  
36 sunrise and solar noon and differences in net energy gains between moorland and forested  
37 sites are minimal. Therefore, the temperature of water crossing the upstream reach boundary  
38 changes little over the day (i.e. heat advected into the reach is reasonably constant) and water  
39 temperature changes at similar rates whether flowing through forest or moorland.  
40 Consequently, minor differences in water temperature are observed throughout the reach.

## 41 **5.3 Limitations**

1 Models are always simplifications of reality and therefore must incorporate assumptions  
2 (Westhoff et al., 2011). Although the model presented herein performed well, a number of  
3 assumptions were made which may have affected its performance. These assumptions are  
4 identified in this section and suggestions are made for future model parameterisation and  
5 application.

6 In using three AWSs situated directly above the stream (one in open moorland and two  
7 within the forest) this study sought to improve upon previous representations of turbulent  
8 heat fluxes where often a single weather station (e.g. Westhoff et al., 2007; 2010; 2011;  
9 Benyahya et al., 2010), sometimes not located within the study catchment (e.g. Westhoff et  
10 al., 2007; Benyahya et al., 2010), has been used. Considerable heterogeneity was observed  
11 between meteorological measurements made at all weather stations, including within the  
12 forest. Consequently, micrometeorological measurements were not only determined by  
13 landuse but also potentially surrounding topography, altitude and aspect. Therefore, it was  
14 considered a reasonable and systematic approach to interpolate values for micrometeorological  
15 variables between AWSs at 1 m intervals. However, this likely introduced some error and  
16 future work should seek to identify methods of more accurately representing  
17 micrometeorological variables, and consequently turbulent fluxes, at high spatial resolution  
18 within stream reaches (particularly forests).

19 Bed heat flux plates connected to each AWS provided aggregated measurements of heat  
20 exchange due to convective, conductive, advective and radiative heat exchanges between the  
21 atmosphere and the riverbed, and the riverbed and the water column (after Evans et al., 1998;  
22 Hannah et al., 2008). Hyporheic exchange should be expected in coarse, highly permeable  
23 gravel-bed rivers such as the Girnock Burn (e.g. Malcolm et al., 2003). Hyporheic exchange  
24 is not considered to have been a major control on the longitudinal patterns observed in this  
25 study since: (1) downstream longitudinal gradients observed at night were very small (i.e. <  
26 0.5 °C) *cf.* daytime, (2) there was no consistent over-prediction of water temperature during  
27 daylight hours, and (3) bed heat flux was minimal at the three sites at which it was measured.  
28 However, it is possible that model errors were due to poor representation of spatially  
29 heterogeneous hyporheic exchange, providing that hyporheic residence times were sufficient  
30 to alter the temperature of re-emerging hyporheic water relative to surface water. Improved  
31 representation of hyporheic exchange processes would involve quantifying: (1) exchange  
32 rates and volumes, (2) residence times, (3) flowpath length and depth, and (4) temperatures of  
33 up- and down-welling hyporheic water throughout the reach. To do this accurately and  
34 represent all flowpaths would be an extremely significant challenge, and efforts to date have  
35 involved a large number of assumptions that could negate the value of estimates of this flux  
36 (e.g. Leach and Moore, 2014). Nevertheless, iterative advances in hyporheic understanding  
37 could progressively improve the predictive power of spatially distributed water temperature  
38 models, especially in the representation of daily temperature variability and lags, depending  
39 on the dominant hyporheic zone processes.

40 Parameters were used in calculations of net radiation and turbulent fluxes. A sensitivity  
41 analysis was conducted on the threshold value used to convert hemispherical photographs  
42 into binary images for radiation modelling; this was possible because measurements of

1 incident shortwave radiation were available to identify representative bounds for this value.  
2 Further parameters used for net radiation modelling were the emissivity of the water, riparian  
3 canopy, and the atmosphere. Emissivity of the riparian canopy and the water were assumed to  
4 be equivalent to values identified during model calibration by Leach and Moore (2010) and  
5 used also by Moore et al. (2005) and MacDonald et al. (2014a, 2014b) for riparian forest  
6 dominated by coniferous trees. Under overcast conditions, emissivity of the atmosphere for  
7 net radiation modelling was dependent on cloud cover for which observational data were  
8 unavailable. An average value for common cloud types (i.e. altostratus, altocumulus,  
9 stratocumulus, stratus and cumulus) was assumed (after Leach and Moore 2010), but may not  
10 have been representative of actual cloud cover conditions. Net radiation model performance  
11 was good in comparison to previous applications (e.g. Leach and Moore, 2010), although we  
12 acknowledge further consideration could be given to the use of emissivity values derived for  
13 forest composed of different vegetation species, and potentially different meteorological  
14 conditions. Turbulent energy exchanges were calculated from micrometeorological  
15 measurements using commonly used methods (e.g. Webb and Zhang, 1997; Hannah et al.,  
16 2004, 2008; Leach and Moore 2010, 2014; MacDonald et al., 2014c; Garner et al., 2014);  
17 these equations are semi-empirical (Ouellet et al., 2014) and thus do contain parameters, but  
18 they are not site-specific. A sensitivity analysis was not performed on these parameters  
19 because in the absence of direct measurements of latent and sensible heat (e.g. Guenther et  
20 al., 2012; Maheu et al., 2014) there was no basis for doing so. Nevertheless, it would have  
21 been beneficial to understand the effects of these parameters on model performance and  
22 future studies may wish to address this.

23 Lastly, the flow routing and water temperature modelling assumed that no significant net  
24 gains or losses of stream flow occurred, and that velocities were uniform throughout the  
25 reach. These assumptions were upheld at locations where flow accretion surveys (plus  
26 previous hydrochemical surveys; Malcolm et al., 2005) and concurrent velocity  
27 measurements were made (i.e. at 200 m intervals throughout the reach). Nevertheless,  
28 unidentified losses and gains to flow could have occurred within the uncertainties of the  
29 gauging approach, and water could have travelled at variable velocities between these survey  
30 locations depending on local channel characteristics. Consequently, it is possible that  
31 discharge and hydraulic retention time within parts of the reach could have been either  
32 increased or reduced, thus allowing enhanced or reduced rates of energy exchange. The good  
33 model performance observed herein suggests that the available data were broadly  
34 representative of conditions throughout the reach. However, the effects of net flow gains and  
35 losses and variable hydraulic retention times warrants further investigation in future studies.

## 36 **6. CONCLUSION**

37 The findings of this study have a number of important implications for researchers and river  
38 managers who may wish to assess the potential for mitigating water temperature extremes  
39 using riparian shading (e.g. riparian planting strategies). Our key finding is that water does  
40 not cool as it flows downstream under a semi-natural forest canopy. Instead, energy gains to  
41 the water column are reduced dramatically in comparison to open landuse, which reduces the



1 rate at which water temperature increases as it travels downstream. Thus, observed  
2 temperatures are controlled by a combination of lagged temperatures from upstream open  
3 reaches and lower rates of temperature increase within the forest. For reaches such as the  
4 Girnock Burn, where upstream landuse does not shade the channel, instantaneous  
5 longitudinal cooling gradients are generated when the temperature of water advected into the  
6 reach increases over the day, while temperature increases are minimal for the water flowing  
7 beneath the forest canopy. This study was conducted under a ‘worst case scenario’ of low  
8 flows and high energy gains; thus under these extreme conditions, cooler stream refugia are  
9 anticipated to be present under forest canopies during daylight hours, but warming of the  
10 water column upstream of the forest will also control absolute water temperatures. Therefore  
11 shading headwater reaches, where water is not in dynamic equilibrium with the atmosphere  
12 (e.g. Erdinger et al., 1968; Hrachowitz et al., 2010; Kelleher et al., 2012; Garner et al., 2013)  
13 and is thus cooler than the majority of locations lower in the basin (Poole and Berman, 2001),  
14 is anticipated to provide cool water refugia for temperature sensitive species and reduce  
15 temperatures further downstream.

16 Under future climates, surface energy balances are anticipated to change (Wild et al., 1997;  
17 Andrews et al., 2008) and discharge in catchments such as the Girnock, which have limited  
18 storage and shorter groundwater residence times, is anticipated to be more variable/ extreme  
19 (Cappel et al., 2013). The water temperature modelling approach used in this study allows  
20 researchers and stream managers to explore the effects of variable prevailing weather and  
21 hydraulic conditions on stream temperatures, and identify optimal locations for the generation  
22 of cooling gradients under different shading regimes under present and future climates.  
23 Future research should utilise tools such as those presented herein to understand the effects of  
24 climate, hydraulic conditions, channel orientation and shading scenarios on water  
25 temperature.

## 26 **AUTHOR CONTRIBUTION**

27 IAM, GG, and DMH designed the study. GG collected field data, wrote the flow-routing  
28 model and the water temperature model scripts, and performed the simulations. GG prepared  
29 the manuscript with input from IAM, JPS, and DMH.

## 30 **ACKNOWLEDGEMENTS**

31 Grace Garner was funded by UK Natural Environment Research Council studentship  
32 NE/1528226/1. Anne Anckorn is thanked for cartographic assistance. Jason Leach and Dan  
33 Moore are thanked for generously sharing their net radiation model script. Nigel Mottram is  
34 thanked for his advice on the water temperature model script. Marine Scotland Science  
35 Freshwater Laboratory staff provided field and technical assistance, maintained and  
36 downloaded weather stations. SEPA provided discharge data. R was used for modelling and  
37 graphics. Martijn Westhoff, two anonymous Reviewers, and Hannah Cloke are thanked for  
38 comments that improved the manuscript.

## 1 REFERENCES

- 2 Andrews, T., Forster, P.M., Gregory, J.M.: A surface energy perspective on climate change.  
3 J. Climate, 22: 2557–2570, 2008.
- 4 Baldocchi, D., Falge, E., Gu, L., Olson, R., Hollinger, D., Running, S., Anthoni, P.,  
5 Bernhofer, C., Davis, K., Evans, R., Fuentes, J., Goldstein, A., Katul, G., Law, B., Lee,  
6 X.H., Malhi, Y., Meyers, T., Munger, W., Oechel, W., Pilegaard, K., Schmid, H.P.,  
7 Valentini, R., Verma, S., Vesala, T., Wilson, K., Wofsy, S.: FLUXNET: A new tool to  
8 study the temporal and spatial variability of ecosystem-scale carbon dioxide, water vapour,  
9 and energy flux densities. Bull. Amer. Meteor. Soc., 11, 2415-2434, 2001
- 10 Bartholow, J. M.: The Stream Segment and Stream network Temperature Models: A Self-  
11 Study Course. US Dept. of the Interior, US Geological Survey, Open-File Report 99-112,  
12 (US), 2000
- 13 Beechie, T., Imaki, H., Greene, J., Wade, A., Wu, H., Pess, G., Roni, P., Kimball, J. and  
14 Stanford, J., Kiffney, P., Mantua, N.: Restoring salmon habitat for a changing climate,  
15 River Res. Appl., 29, 939-960, 2013.
- 16 Beschta, R. L. and Taylor R. L.: Stream temperature increases and land use in a forested  
17 Oregon watershed, Water Resour. Bull., 24, 19-25, 1988.
- 18 Boyd, M., Kasper, B.: Analytical methods for dynamic open channel heat and mass transfer:  
19 Methodology for heat source model Version 7.0. Oregon Department of Environmental  
20 Quality, 2003
- 21 Brown, G.W., Swank, G.W., and Rothacher, J.: Water temperature in the Steamboat  
22 Drainage, USDA For. Serv. Res. Pap. PNW-119, 1971.
- 23 Brown, L.E., Cooper, L., Holden, J. and Ramchunder S.J.: A comparison of stream water  
24 temperature regimes from open and afforested moorland, Yorkshire Dales, northern  
25 England, Hydrol. Processes, 24, 3206-3218, 2010.
- 26 Burnham, K.P. and Anderson, D.R.: Model Selection and Multimodel Inference: A Practical  
27 Information-Theoretic Approach. New York: Springer . 480, 2002.
- 28 Caissie, D.: The thermal regime of rivers: a review. Freshwater Biol., 51, 1389-1406, 2006.
- 29 Cappel, R., Tetzlaff, D. and Soulsby, C.: Will catchment characteristics moderate the  
30 projected effects of climate change on flow regimes in the Scottish Highlands? Hydrol.  
31 Processes, 27, 687-699, 2013.
- 32 Cozzetto, K., McKnight D., Nysten, T., Fountain, A.: Experimental investigations into  
33 processes controlling stream and hyporheic temperatures, Fryxell Basin, Antarctica, Adv.  
34 Water Res., 29, 130-153, 2006.
- 35 Danehy, R.J., Colson, C.G., Parrett, K.B. and Duke, S.D.: Patterns and sources of thermal  
36 heterogeneity in small mountain streams within a forested setting, Forest Ecol. Manag,  
37 208, 287–302, 2005.
- 38 Edinger, J.E., Duttweiler, D.W. and Geyer, J.C.: The response of water temperatures to  
39 meteorological conditions. Water Resour. Res. 4, 1137–1143, 1968.
- 40 Evans, E.C., McGregor, G.R., Petts, G.E.: River energy budgets with special reference to  
41 riverbed processes, Hydrol. Processes, 12, 575-595, 1998.
- 42 Frazer, G.W., Canham, C.D. and Lertzman, K.P.: Gap Light Analyser (GLA), Version 2:  
43 Imaging Software to Extract Canopy Structure and Light Transmission Indices from True-  
44 Colour Fisheye Photographs. User's Manual and Program Documentation. Simon Fraser  
45 University and the Institute of Ecosystem Studies, Millbrook (NY), 36, 1999.

- 1 Garner, G., Malcolm, I. A., Sadler, J.P., Millar, C. P. and Hannah, D. M.: Inter-annual  
2 variability in the effects of riparian woodland on micro-climate, energy exchanges and  
3 water temperature of an upland Scottish stream, *Hydrol. Processes*, DOI:  
4 10.1002/hyp.10223, 2014.
- 5 Garner, G., Hannah, D.M., Sadler, J.P. and Orr, H.G.: River temperature regimes of England  
6 and Wales: spatial patterns, inter-annual variability and climatic sensitivity, *Hydrol.*  
7 *Processes*, DOI: 10.1002/hyp.9992, 2013.
- 8 Gomi, T., Moore, R.D. and Dhakal, A.S.: Headwater stream temperature response to clear-  
9 cut harvesting with different riparian treatments coastal British Columbia Canada, *Water*  
10 *Resour. Res.*, 42, DOI: 10.1029/2005WR004162, 2006.
- 11 Guenther, S.M., Moore, R.D., Gomi, T.: Riparian microclimate and evaporation from a  
12 coastal headwater stream, and their response to partial-retention forest harvesting, *Agr*  
13 *Forest Meteorol.*, 161 1-9, 2012.
- 14 Hannah, D.M., Malcolm, I.A. and Bradley, C.: Seasonal hyporheic temperature dynamics  
15 over riffle bedforms. *Hydrol. Processes*, 15, 2178-2194, 2009.
- 16 Hannah, D.M., Malcolm, I.A., Soulsby, C. and Youngson, A.F.: Heat exchanges and  
17 temperatures within a salmon spawning stream in the Cairngorms, Scotland: seasonal and  
18 sub-seasonal dynamics. *River Res. App.*, 22, 919-940, 2004.
- 19 Hannah, D.M., Malcolm, I.A., Soulsby, C. and Youngson, A.F.: A comparison of forest and  
20 moorland stream microclimate, heat exchanges and thermal dynamics, *Hydrol. Processes*,  
21 22, 919-940, 2008.
- 22 Hastie, T.J. and Tibshirani, R.J.: Generalized additive models. *Stat. Science.* 1, 297-318.  
23 1986.
- 24 Hrachowitz, M., Soulsby, C., Imholt, C., Malcolm, I.A. and Tetzlaff, D.: Thermal regimes in  
25 a large upland salmon river: a simple model to identify the influence of landscape controls  
26 and climate change on maximum temperatures, *Hydrol. Processes*, 24, 3374-3391, 2010..
- 27 Imholt, C., Gibbins, C.N., Malcolm, I.A., Langan, S., Soulsby, C.: Influence of riparian tree  
28 cover on stream temperatures and the growth of the mayfly *Baetis rhodani* in an upland  
29 stream, *Aquat. Ecol.*, 44, 669-678, 2010.
- 30 Imholt, C., Soulsby, C., Malcolm, I.A., Gibbins, C.N.: Influence of contrasting riparian forest  
31 cover on stream temperature dynamics in salmonid spawning and nursery streams,  
32 *Ecohydrology*, 6, 380-392, DOI: 10.1002/eco.1291, 2012.
- 33 Iqbal, M.: An Introduction to Solar Radiation, Academic Press: Toronto, 390, 1983.
- 34 Johnson, S.L. and Jones, J.A.: Stream temperature responses to forest harvest and debris  
35 flows in Western Cascades Oregon, *Can. J. Fish. Aquat. Sci.*, 57, 30-39, 2000.
- 36 Keith, R.M., Bjornn, T.C., Meehan, W.R., Hetrickm J. and Brusvenn, M.A.: Response of  
37 juvenile salmonids to riparian and instream cover modifications in small streams flowing  
38 through second-growth forests of south-east Alaska, *T Am Fish Soc.*, 127, 899-907, 1998.
- 39 Kelleher, C., Wagener, T., Gooseff, M., McGlynn, B., McGuire, K., Marshall, L.:  
40 Investigating controls on the thermal sensitivity of Pennsylvania streams, *Hydrol.*  
41 *Processes*, 26, 771-785, 2012.
- 42 Leach, J.A. and Moore, R.D.: Above-stream microclimate and stream surface energy  
43 exchanges in a wildfire distributed zone, *Hydrol. Processes*, 24, 2369-2381, 2010.

- 1 Leach, J.A. and Moore, R.D.: Stream temperature dynamics in two hydrogeomorphically  
2 distinct reaches, *Hydrol. Processes*, 25, 679-690, 2011.
- 3 Leach, J.A., Moore, R.D., Hinch, S.G. and Gomi, T.: Estimation of logging-induced stream  
4 temperature changes and bioenergetic consequences for cutthroat trout in a coastal stream  
5 in British Columbia, Canada, *Aquat. Sci.* 74, 427441, 2012.
- 6 Leach, J.A., Moore, R.D.: Winter stream temperature in the rain-on-snow zone of the Pacific  
7 Northwest: influences of hillslope runoff and transient snow cover, *Hydrol. Earth Syst.*  
8 *Sci.*, 8, 819-838, 2014.
- 9 Macdonald, J.S., MacIsaac, E.A., Heurer, H.E.: The effect of variable retention riparian  
10 buffer zones on water temperatures in small headwater streams in sub-boreal forest  
11 ecosystems of British Columbia. *Can. J. Forest Res.*, 33, 303-316, 2003.
- 12 MacDonald, R.J., Boon, S., Byrne, J.M., Robinson, M.D. and Rasmussen, J.B.: Potential  
13 future climate effects on mountain hydrology, stream temperature and native salmon  
14 history. *Can. J. Fish. Aquat. Sci.*, 71, 189-202, 2014a.
- 15 MacDonald, R.J., Boon, S., Byrne, J.M., Silins, U.: A process-based stream temperature  
16 modelling approach for mountain regions, *J. Hydrol*, 511, 920-931, 2014b.
- 17 MacDonald, R.J., Boon, S., Byrne, J.M., Silins, U.: A comparison of surface and subsurface  
18 controls on summer temperature in a headwater stream, *Hydrol. Processes*, 28, 2338-2347,  
19 2014c.
- 20 [Maheu, A., Caissie, D., St-Hilaire, A., El-Jabi, N.: River evaporation and corresponding heat  
21 flux in forested catchments, \*Hydrol. Processes\*, 28, 5725-5738, 2014.](#)
- 22 Malcolm, I.A., Hannah, D.M., Donaghy, M.J., Soulsby, C. and Youngson, A.F.: The  
23 influence of riparian woodland on the spatial; and temporal variability of stream water  
24 temperatures in an upland salmon stream, *Hydrol. Earth Syst. Sci.*, 8, 449-459, 2004.
- 25 Malcolm, I.A., Soulsby, C., Hannah, D.M., Bacon, P.J., Youngson, A.F. and Tetzlaff D.: The  
26 influence of riparian woodland on stream temperatures: implications for the performance  
27 of juvenile salmonids, *Hydrol. Processes*, 22, 968-979, 2008.
- 28 Malcolm, I.A., Soulsby, C., Youngson, A.F. and Hannah, D.M: Catchment scale controls on  
29 groundwater-surfacewater interactions in the hyporheic zone: implications for salmon  
30 embryo survival, *River Res. App.*, 21, 977-989, 2005.
- 31 Malcolm, I.A., Youngson, A.F., Soulsby, C.: Survival of salmonid eggs in a degraded in a  
32 degraded gravel-bed stream: effects of groundwater-surface water interactions, *River Res.*  
33 *App.*, 19, 303-316, 2003.
- 34 McGurk, B.J.: Predicting stream temperature after riparian vegetation removal, in:  
35 *Proceedings of the Californian Riparian Systems Conference: Protection, Management*  
36 *and Restoration for the 1990s*, 22-24 September 1988, Davis, California, 1988.
- 37 Moore, R.D., Sutherland, P., Gomi, T. and Dakal, A.: Thermal regime of a headwater stream  
38 within a clear-cut, coastal British Columbia, *Hydrol. Processes*, 19, 2591-2608, 2005.
- 39 Moore, R.D., Leach, J.A., Knudson, J.M.: Geometric calculation of view factors for stream  
40 surface radiation modelling in the presence of riparian forest, *Hydrol. Processes*, 28, 2975-  
41 2986, 2014.
- 42 Ouellet, V., Secretan, Y., St-Hilaire, A., Morin, J.: Water temperature modelling in a  
43 controlled environment: comparative study of heat budget equations, *Hydrol. Processes*,  
44 28, 279-292, 2014

1 Prata, A.J.: A new long-wave formula for estimating downward clear-sky radiation at the  
2 surface, *Q. J. Roy. Meteor. Soc.*, 122, 1127–1151, 1996.

3 Poole, G.C. and Berman C.H.: An ecological perspective on in-stream temperature : natural  
4 heat dynamics and mechanisms human-caused thermal degradation, *Environ. Manage.*, 27,  
5 787-802, 2001.

6 R Core Team, R: A Language and Environment for Statistical Computing. R Foundation for  
7 Statistical Computing: Vienna, Austria: <http://www.R-project.org>, 2013.

8 Roth, T.R., Westhoff, M.C., Huwald, H., Huff, J.A., Rubin, J.F., Barrenetxea, G., Vetterli, G.,  
9 Parriaux, A., Selker, J.S., Parlange, M.B.: Stream temperature response to three riparian  
10 planting scenarios by use of a distributed temperature validated model, *Environ. Sci.*  
11 *Technol.*, 44, 2072-2078, 2010.

12 Rutherford, J.C., Blackett, S., Blackett, C., Saito, L. and Davies-Colley, R.K.: Predicting the  
13 effects of shade on water temperature in small streams, *New Zeal. J. Mar. Fresh.*, 31, 707-  
14 721, 1997.

15 Rutherford, J.C., Marsh, N.A., Davies, P.M. and Bunn, S.E.: Effects of patchy shade on  
16 stream water temperature: how quickly do small streams heat and cool?, *Mar. Freshwater*  
17 *Res.*, 55, 737-748, 2004.

18 Story, A., Moore, R.D. and MacDonald, J.S.: Stream temperatures in two shaded reaches  
19 below cutblocks and logging roads: downstream cooling linked to subsurface hydrology,  
20 *Can. J. Forest Res.*, 33, 1383-1396, 2003.

21 Soetaert, K., Petzoldt, T., Woodrow Setzer, R.: Solving Differential Equations in R: Package  
22 deSolve, *J. Stati. Softw.* 33, 1–25, 2010.

23 Tetzlaff, D., Soulsby, C., Gibbins, C., Bacon, P.J., Youngson, A.F: An approach to assessing  
24 hydrological influences on feeding opportunities of juvenile Atlantic salmon (*Salmo*  
25 *salar*): a case study of two contrasting years in a small, nursery stream, *Hydrobiologia*,  
26 549, 65-77, 2005.

27 Tetzlaff, D., Soulsby, C., Waldron, S., Malcolm, I.A., Bacon, P.J., Dunn, S.M., Lilly, A. and  
28 Youngson, A.F.: Conceptualisation of runoff processes using a geographical information  
29 system and tracers in a nested mesoscale catchment., *Hydrol. Processes*, 21, 1289-1307,  
30 2007.

31 Upper Dee riparian scheme, The River Dee Trust:  
32 [http://www.theriverdeetrust.org.uk/information/our\\_work.asp](http://www.theriverdeetrust.org.uk/information/our_work.asp), last accessed: 24/04/214,  
33 2011.

34 Torgerson, C.E., Price, D.M., Li, H.W. and McIntosh, B.A.: Multiscale thermal refugia and  
35 stream habitat associations of chinook salmon in northeastern Oregon. *Ecol. App.*, 9, 301–  
36 319, 1999.

37 van Vliet, M.T.H., Ludwig, F., Zwolsman, J.J.G., Weedon, G.P. and Kabat, P.: Global river  
38 temperatures and sensitivity to atmospheric warming and changes in river flow, *Water*  
39 *Res. Res.*, 47, doi:10.1029/2010WR009198, 2011.

40 Webb, B.W., Hannah, D.M., Moore, R.D., Brown, L.E. and Nobilis, F.: Recent advances in  
41 stream and river temperature research, *Hydrol. Processes*, 22, 902-918, 2008.

42 Webb, B.W. and Zhang, Y.: Spatial and seasonal variability in the components of the river  
43 heat budget, *Hydrol. Processes*, 11, 79-101, 1997.

44 Westhoff, M.C., Savenije, H.H.G., Luxemburg, W.M.G., Stelling, G.S., van de Giessen,  
45 N.C., Selker, J.S., Pfister, L., Uhlenbrook, S.: A distributed stream temperature model  
46 using high resolution temperature observations, 4, 1469-1480, 2007.

- 1 Westhoff, M.C., Bogaard, T.A., Savenije, H.H.G.: Quantifying the effect of in-stream rock  
2 clasts on the retardation of heat along a stream, 11, 1417-1425, 2010.
- 3 Westhoff, M.C., Gooseff, M.N., Bogaard, T.A., Savenije, H.G.G., Quantifying hyporheic  
4 exchange at high spatial resolution using natural temperature variations along a first-order  
5 stream, *Hydrol. Earth Syst. Sci.*, 47, DOI: 10.1029/2010WR009767, 2011.
- 6 Wilby, R.L., Orr, H.G., Watts, G., Battarbee, R.W., Berry, P.M., Chadd, R., Dugdale, S.J.,  
7 Dunbar, M.J., Elliott, J.A., Extence, C., Hannah, D.M., Holmes, N., Johnson, A.C.,  
8 Knights, B., Milner, N.J., Ormerod, S.J., Solomon, D., Timlett, R., Whitehead, J. and  
9 Wood P.J.: Evidence needed to manage freshwater ecosystems in a changing climate:  
10 turning adaptation principles into practice, *Sci. Tot. Environ.*, 408, 4150-4164, 2010.
- 11 Wild, M., Ohmura, A. and Cubasch, U.: GCM-simulated energy fluxes in climate change  
12 experiments. *J. Climate*, 10, 3093-3110, 1997.
- 13 Wood, S.N.: *Generalized additive models: an introduction with R*, Boca Raton. Chapman and  
14 Hall/CRC, Boca Raton, 391, 2006.
- 15 Yearlsey, J.R.: A semi-Lagrangian water temperature model for advection-dominated river  
16 systems, *Water Res. Res.*, 45, doi: 10.1029/2008WR007629, 2009.
- 17 Zwieniecki, M. and Newton, M.: Influence of streamside cover and stream features on  
18 temperature trends in forested streams of western Oregon, *West. J. Appl. For.* 14, 106–  
19 112, 1999.

1 **FIGURE CAPTIONS**

2 Figure 1. (a) Location map of the Girnock (b) Girnock catchment (c) locations of field data  
3 collection.

4 Figure 2. Study period (a) air temperature (b) discharge, and energy fluxes at (c)  $AWS_{Open}$  (d)  
5  $AWS_{FUS}$  (e)  $AWS_{FDS}$ , (f) and water temperature at  $AWS_{Open}$ ,  $AWS_{FDS}$  and  $AWS_{Open}$  minus  
6  $AWS_{FDS}$  (positive values indicate that temperature  $AWS_{Open}$  was greater than temperature at  
7  $AWS_{FDS}$ ). Averages represent values for DOYs 183 to 289 in the 10 years preceding 2013.

8 Figure 3. Instantaneous stream temperature gradients during field data collection. Positive  
9 values indicate that temperature at  $AWS_{Open}$  was greater than that at  $AWS_{FDS}$  (i.e.  
10 instantaneous cooling gradient) while positive values indicate that temperature at  $AWS_{Open}$   
11 was less than that at  $AWS_{FDS}$  (i.e. instantaneous warming gradient).

12 Figure 4. Spatio-temporal patterns in instantaneous water temperature measurements (a)  
13 absolute values ( $^{\circ}C$ ) and (b) differences between  $AWS_{Open}$  and each monitoring location  
14 within the reach (positive values indicate instantaneous cooling gradients). Values for both  
15 panels were interpolated linearly at 1 m intervals from observations.

16 Figure 5. Hemispherical photographs representative of (a) clear sky view (b) low density,  
17 patchy riparian forest (c) low density, continuous riparian forest (d) high density, continuous  
18 riparian forest. The grid represents the  $5^{\circ}$  azimuth and zenith overlay applied by Gap Light  
19 Analyser software.

20 Figure 6. Patterns within the reach in (a) canopy density. Points indicate spot observations of  
21 canopy density obtained from hemispheric photographs. Solid line indicates smoothed  
22 downstream trends (b) net energy flux ( $MJm^2d^{-1}$ ).

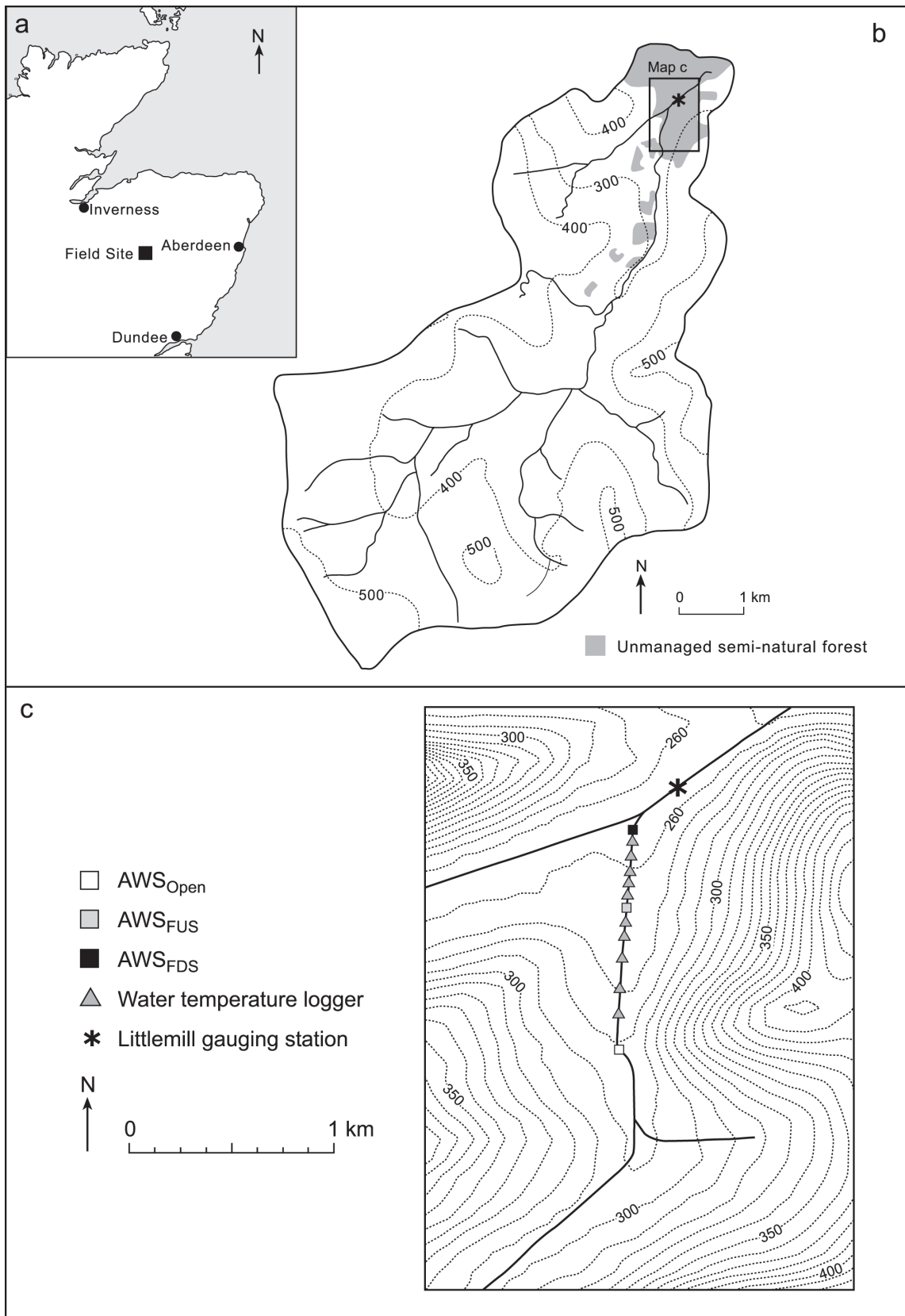
23 Figure 7: Observed and modelled water temperature at  $AWS_{FDS}$

24 Figure 8. Modelled (lines) and observed (points) water temperatures of parcels released from  
25  $AWS_{Open}$  at hourly intervals between 06:00 and 09:00 GMT on each day of the study period.  
26 Grey envelopes demonstrate the influence of the threshold parameter used to convert  
27 hemispherical photographs to binary images prior to incident solar radiation modelling.  
28 Lower bound is representative of the maximum threshold value; upper bound is  
29 representative of the minimum threshold value.

30 Figure 9. Temperature of water parcels (black lines on the date and time axis) routed through  
31 the reach from  $AWS_{Open}$  at hourly intervals (a) on day six (b) day two

32

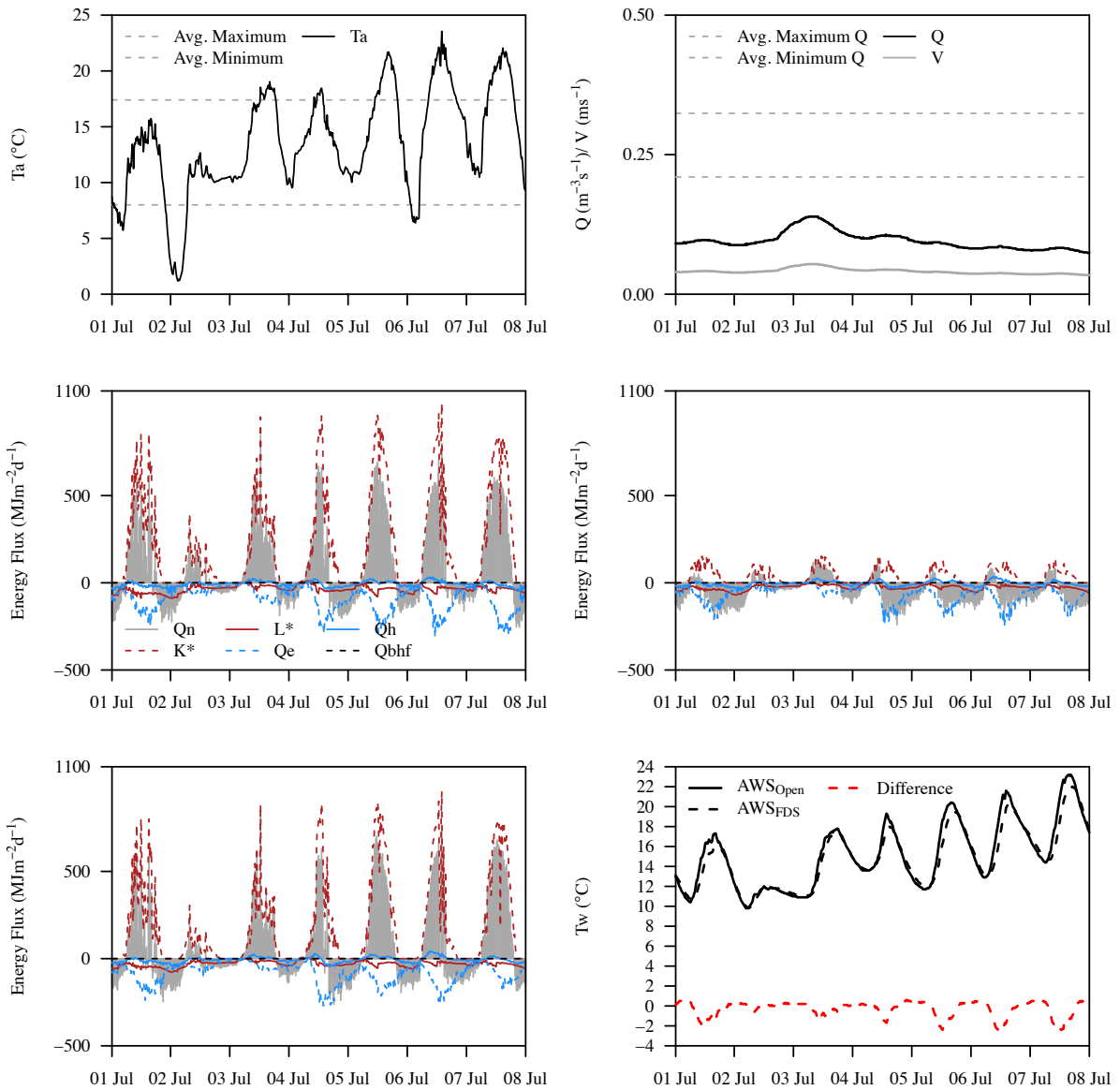
1 FIGURES



2

3 **Figure 1.** (a) Location map of the Girmock (b) Girmock catchment (c) locations of field data collection.  
4





2

3

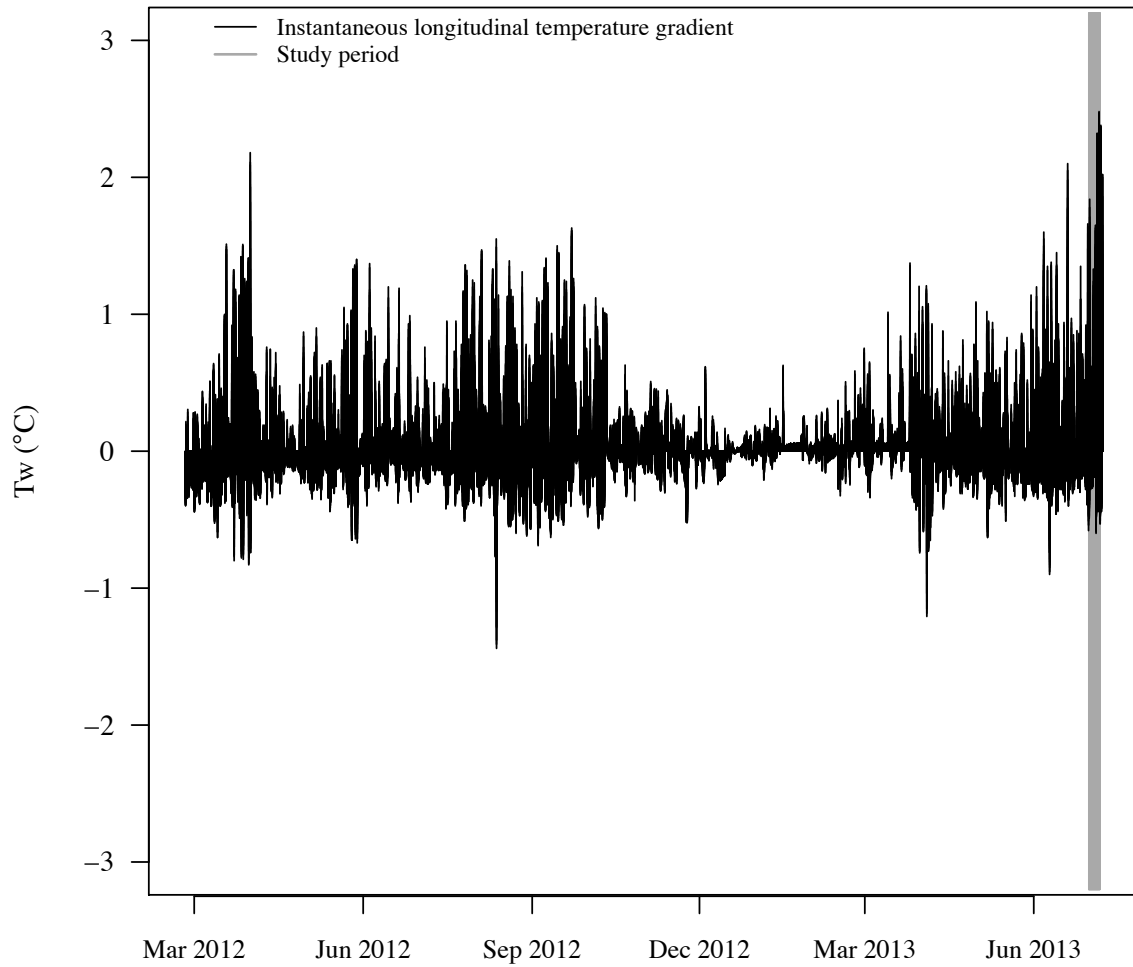
4

5

6

7

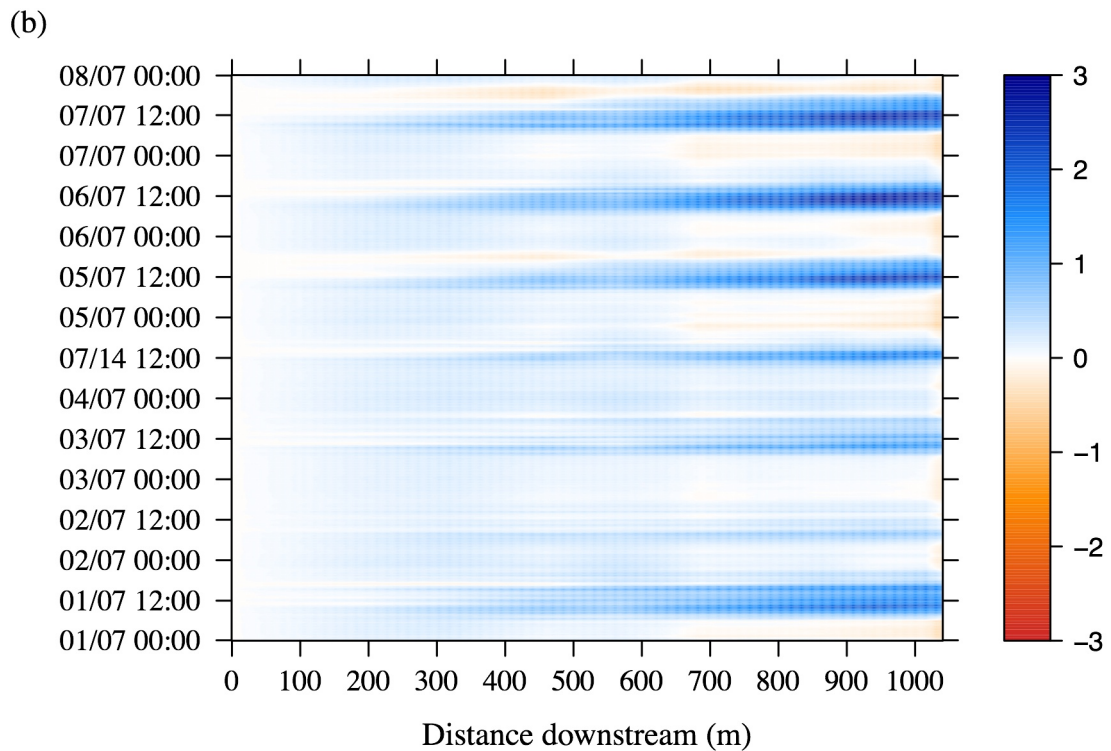
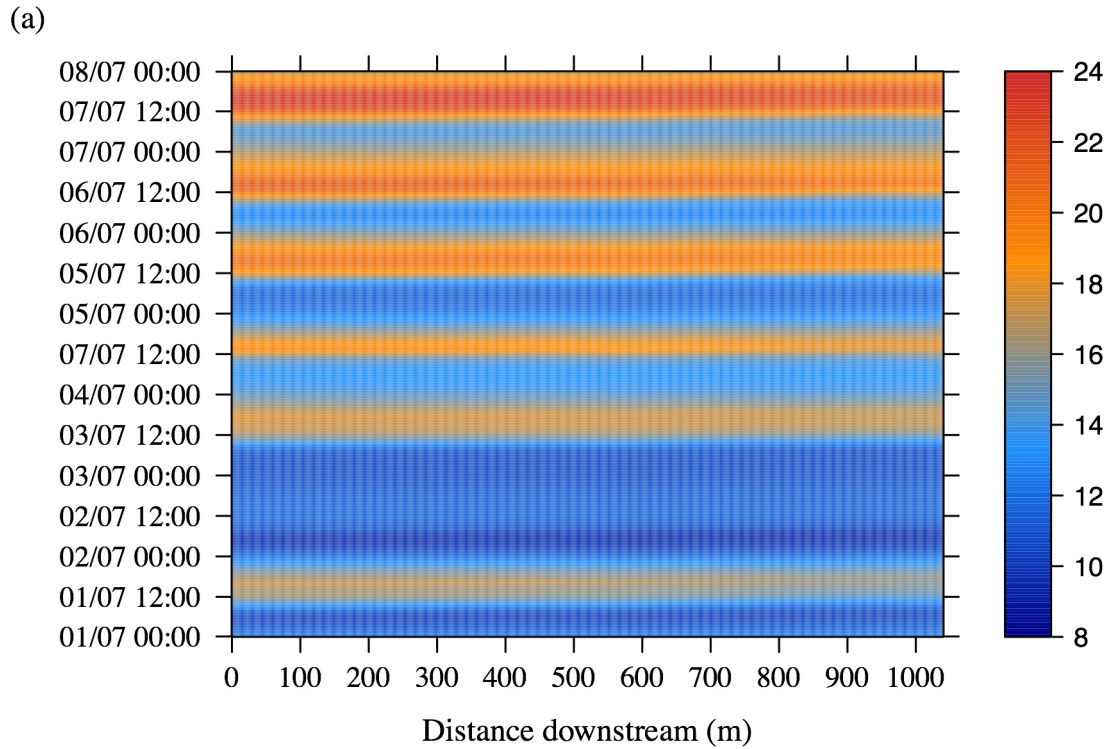
**Figure 2.** Study period (a) air temperature (b) discharge, and energy fluxes at (c)  $\text{AWS}_{\text{Open}}$  (d)  $\text{AWS}_{\text{FUS}}$  (e)  $\text{AWS}_{\text{FDS}}$ , (f) and water temperature at  $\text{AWS}_{\text{Open}}$ ,  $\text{AWS}_{\text{FDS}}$  and  $\text{AWS}_{\text{Open}}$  minus  $\text{AWS}_{\text{FDS}}$  (positive values indicate that temperature  $\text{AWS}_{\text{Open}}$  was greater than temperature at  $\text{AWS}_{\text{FDS}}$ ). Averages represent values for DOYs 183 to 289 in the 10 years preceding 2013.



1

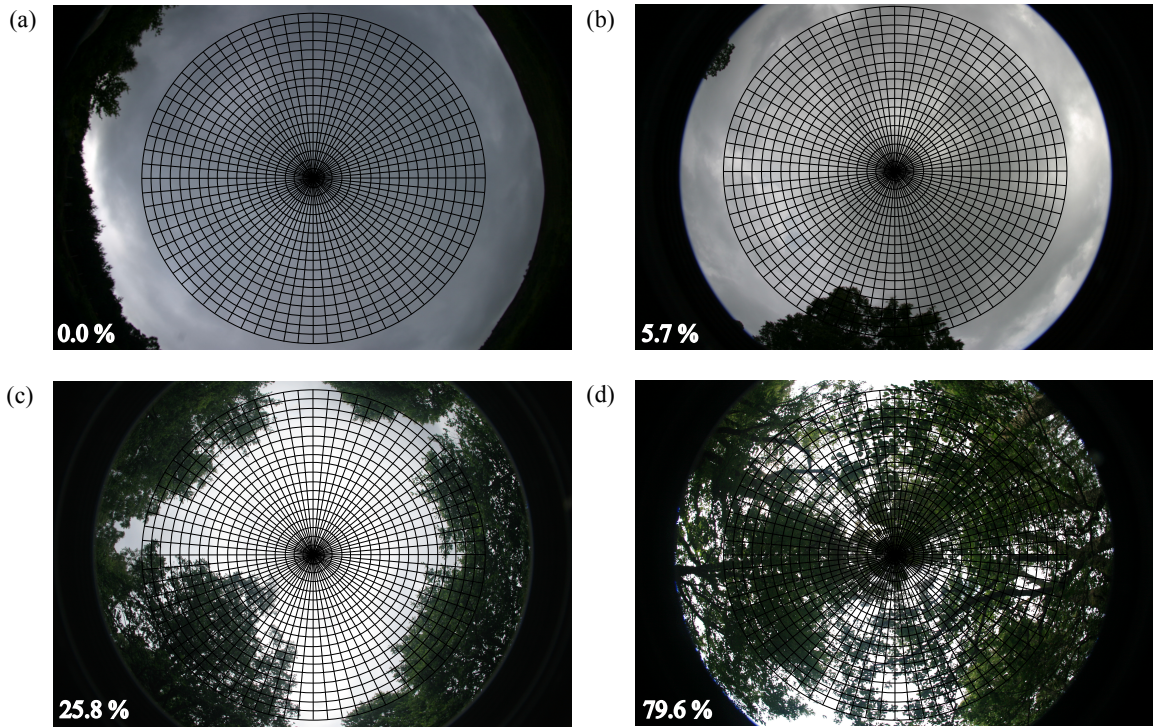
2 **Figure 3.** Instantaneous stream temperature gradients during field data collection. Positive values  
 3 indicate that temperature at  $AWS_{Open}$  was greater than that at  $AWS_{FDS}$  (i.e. instantaneous cooling  
 4 gradient) while positive values indicate that temperature at  $AWS_{Open}$  was less than that at  $AWS_{FDS}$  (i.e.  
 5 instantaneous warming gradient).

6



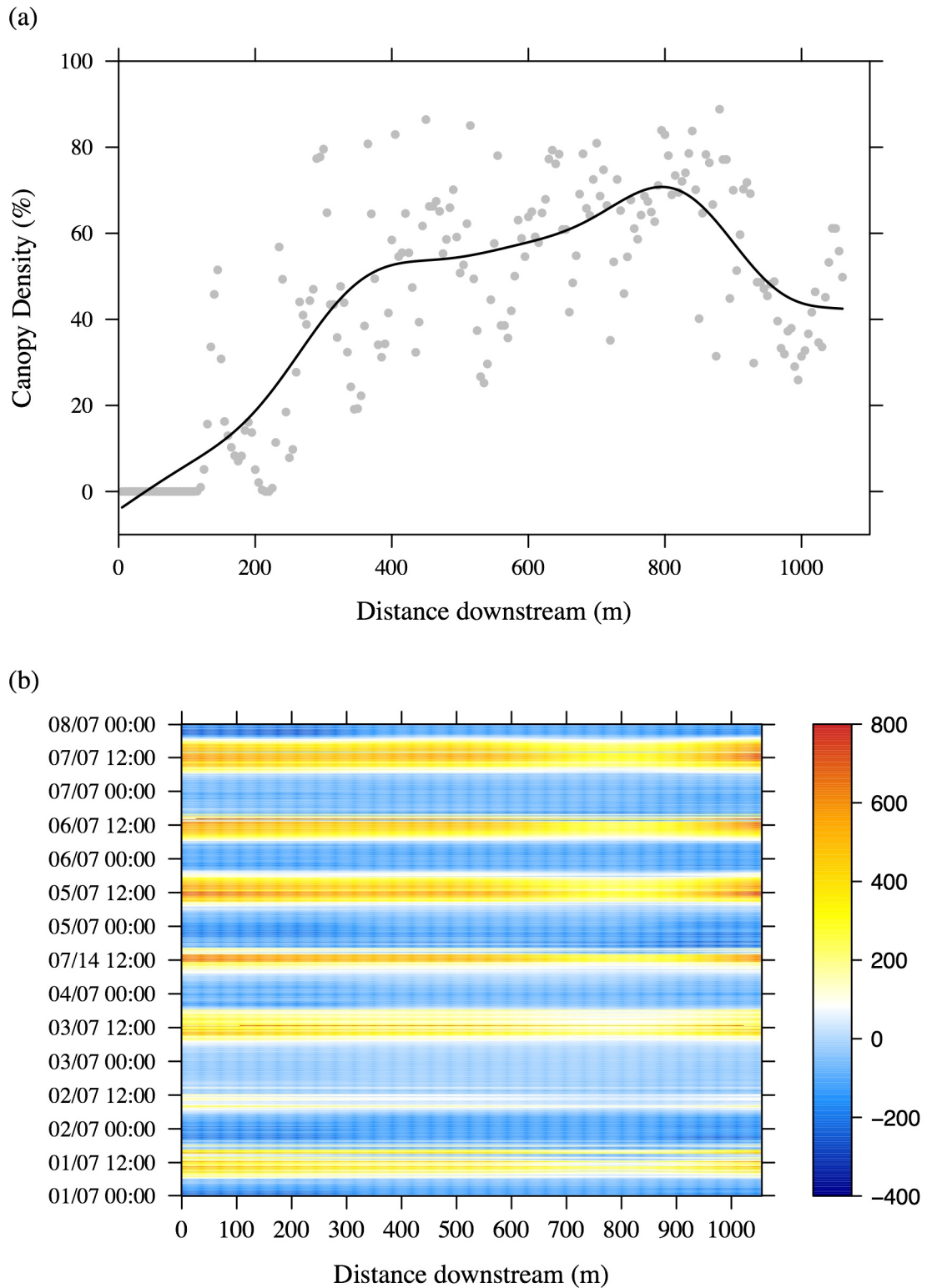
1  
2  
3  
4  
5  
6

**Figure 4.** Spatio-temporal patterns in instantaneous water temperature measurements (a) absolute values ( $^{\circ}\text{C}$ ) and (b) differences between  $\text{AWS}_{\text{Open}}$  and each monitoring location within the reach (positive values indicate instantaneous cooling gradients). Values for both panels were interpolated linearly at 1 m intervals from observations.



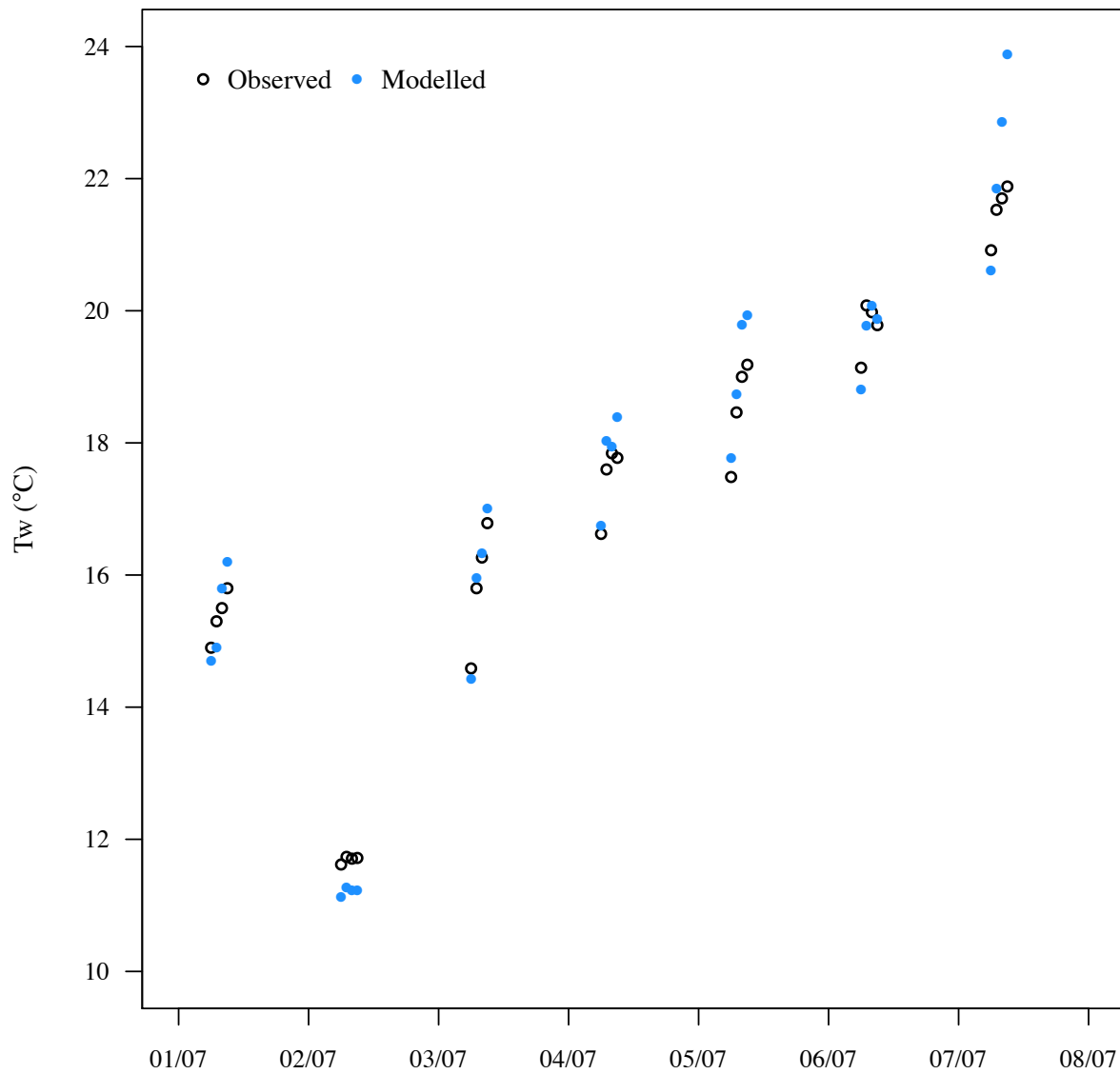
1  
 2 **Figure 5.** Hemispherical photographs representative of (a) clear sky view (b) low density, patchy  
 3 riparian forest (c) low density, continuous riparian forest (d) high density, continuous riparian forest.  
 4 The grid represents the 5 ° azimuth and zenith overlay applied by Gap Light Analyser software.

5



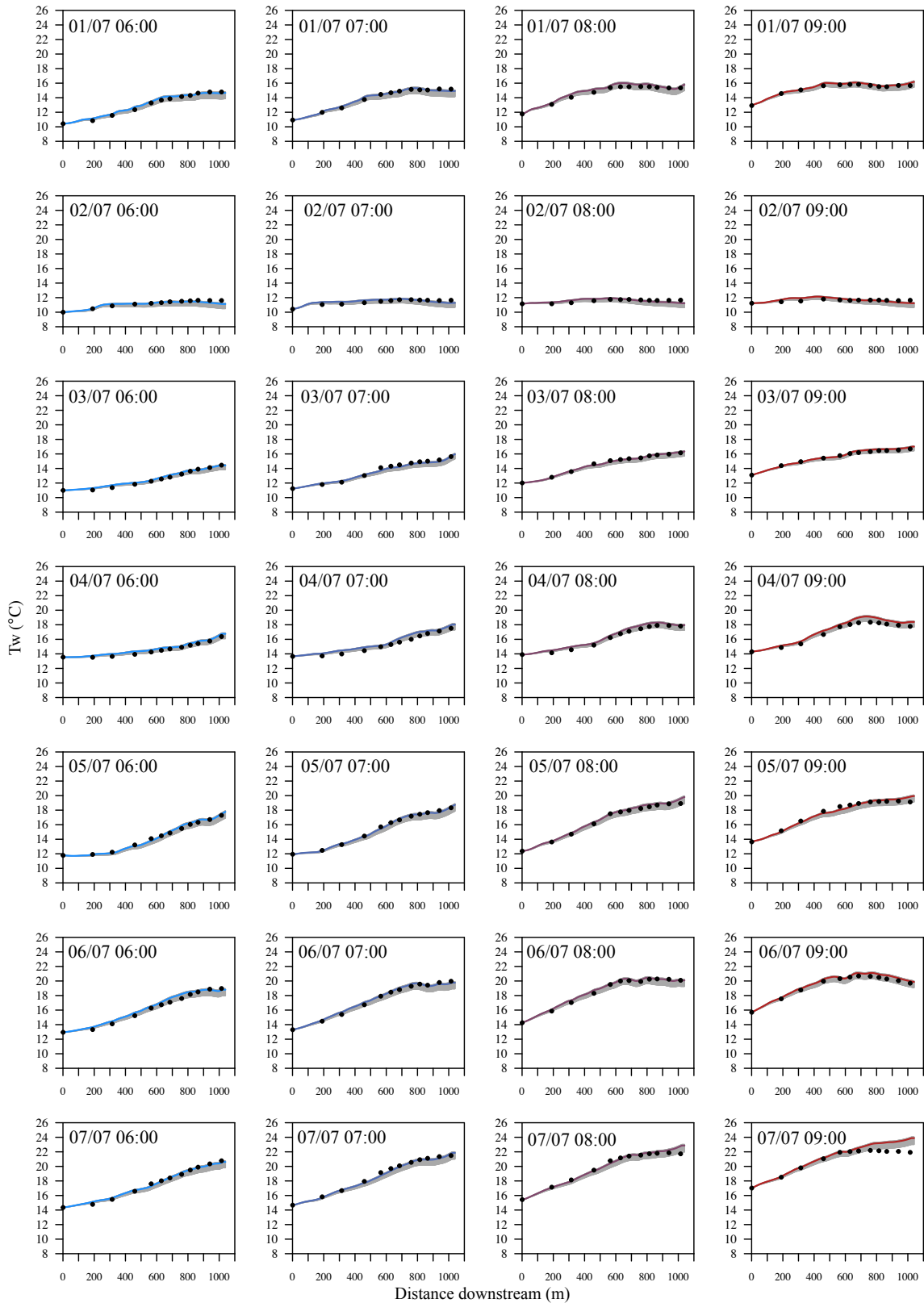
1

2 **Figure 6.** Patterns within the reach in (a) canopy density. Points indicate spot observations of  
 3 canopy density obtained from hemispheric photographs. Solid line indicates smoothed  
 4 downstream trends (b) net energy flux ( $\text{MJm}^2\text{d}^{-1}$ ).



1  
2  
3

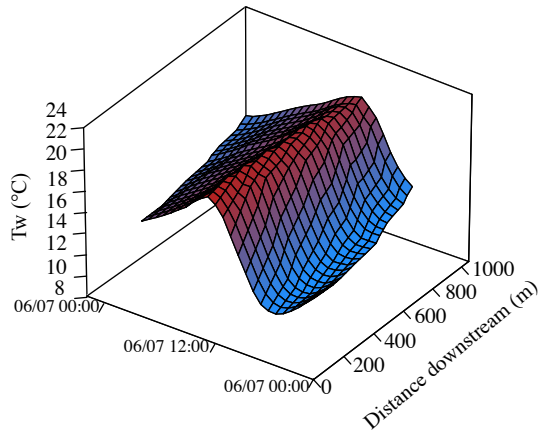
**Figure 7:** Observed and modelled water temperature at  $AWS_{FDS}$



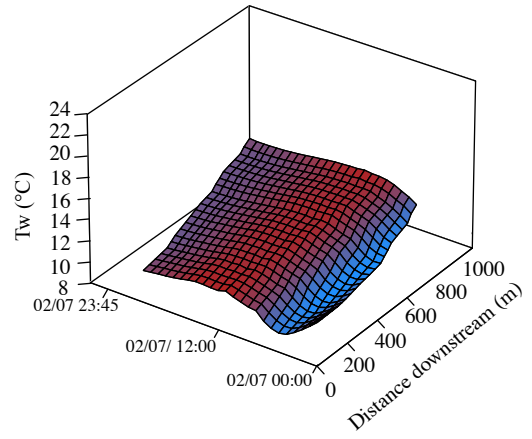
1  
2  
3  
4  
5  
6  
7

**Figure 8.** Modelled (lines) and observed (points) water temperatures of parcels released from  $AWS_{Open}$  at hourly intervals between 06:00 and 09:00 GMT on each day of the study period. Grey envelopes demonstrate the influence of the threshold parameter used to convert hemispherical photographs to binary images prior to incident solar radiation modelling. Lower bound is representative of the maximum threshold value; upper bound is representative of the minimum threshold value.

(a)



(b)



1

2 **Figure 9.** Temperature of water parcels (black lines on the date and time axis) routed through the  
3 reach from AWS<sub>Open</sub> at hourly intervals